European Journal of Medicinal Chemistry 187 (2020) 111961

Contents lists available at ScienceDirect

European Journal of Medicinal Chemistry

journal homepage: http://www.elsevier.com/locate/ejmech

Research paper

Usnic acid derivatives as tau-aggregation and neuroinflammation inhibitors

Cun-Jian Shi, Wan Peng, Jin-Hua Zhao, Hua-Li Yang, Lai-Liang Qu, Cheng Wang, Ling-Yi Kong**, Xiao-Bing Wang*

Jiangsu Key Laboratory of Bioactive Natural Product Research and State Key Laboratory of Natural Medicines, Department of Natural Medicinal Chemistry, School of Traditional Chinese Pharmacy, China Pharmaceutical University, Nanjing, 210009, China

ARTICLE INFO

Article history:
Received 21 November 2019
Received in revised form
9 December 2019
Accepted 9 December 2019
Available online 12 December 2019

Keywords:
Alzheimer's disease
Usnic acid derivatives
Tau anti-aggregation
Anti-inflammatory

ABSTRACT

Accumulation of tau protein aggregation plays a crucial role in neurodegenerative diseases, such as Alzheimer's disease (AD). Uncontrollable neuroinflammation and tau pathology form a vicious circle that further aggravates AD progression. Herein, we reported the synthesis of usnic acid derivatives and evaluation of their inhibitory activities against tau-aggregation and neuroinflammation. The inhibitory activity of the derivatives against the self-fibrillation of the hexapeptide AcPHF6 was initially screened by ThT fluorescence assay. Using circular dichroism and transmission electron microscopy, compound **30** showed the most potent inhibitory activity against AcPHF6 self-fibrillation. Compound **30** was further confirmed to inhibit the aggregation of full-length 2N4R tau protein by a heparin-induced mechanism. In addition, we investigated the anti-inflammatory activity of compound **30,** and showed that compared with sodium usnate, it reduced NO release in LPS-stimulated mouse microglia BV2 cells. More importantly, **30** showed significant protective effects against okadaic acid-induced memory impairment in rats. Thus, **30** was a novel tau-aggregation and neuroinflammation inhibitor that represented a potential therapeutic candidate for AD.

1. Introduction

Alzheimer's disease (AD), a neurodegenerative disease and the most common form of dementia, is characterized by senile plaques formed by amyloid-β (Aβ) outside neurons in the brain and neurofibrillary tangles (NFTs) consisting of hyperphosphorylated-tau inside neurons [1,2]. This abnormal accumulation and misfolding of proteins exacerbate the damage and death of neurons [3,4]. In addition, oxidative stress [5], neuroinflammation [6], metal ion disorders [7], and low level of abnormal deposition acetylcholine (ACh) [8] can also lead to the pathology of AD. Owing to the complexity of the pathological mechanism of AD, researchers propose that the cure of a single target is not realistic [9]. Although multitarget-directed ligands (MTDLs) have made great progress [10], there are still no drugs available for treating AD. Obviously, selection of appropriate targets is of utmost importance.

Aβ hypothesis still occupies a predominant place in pharmaceutical product pipelines (either single or multitarget). According to a scientific data list, in 2018, drugs addressing Aβ targets accounted for 54% of the AD drugs in phase III clinical trials [11]. Nevertheless, all drugs targeting Aβ have failed, and this hypothesis has been questioned [12]. One explanation is that Aβ may not be particularly harmful in itself, but induces tau hyperphosphorylation and enhances tau-seeded pathology, and finally exerts further negative effects [13]. Some findings have suggested that the pathological development of tau is more related to the degree of cognitive impairment than to Aβ [14,15]. In addition, tau imaging is also superior to Aβ imaging in predicting the progression and status of AD [16,17]. All these findings indicate that tau is a more meaningful target of AD than Aβ.

Tau, a microtubule-associated protein predominantly expressed in nerve cells, has an important role in microtubule assembly and stabilization [18,19]. In fact, natively unfolded tau is highly soluble and shows little tendency for aggregation. In pathological conditions, both kinase activation (e.g. glycogen synthase kinase-3β, GSK-3β) and phosphatase inhibition (e.g. protein phosphatase 2A, PP2A) are able to hyperphosphorylate tau, which detach from

* Corresponding author.
** Corresponding author.
E-mail addresses: cpu_lykong@126.com (L.-Y. Kong), xbwang@cpu.edu.cn (X.-B. Wang).

https://doi.org/10.1016/j.ejmech.2019.111961
0223-5234/

microtubules easily and tends to aggregate into neurotoxic NTFs [4,20–22]. Correspondingly, microtubules are depolymerized and subsequently lose their function owing to the shedding of tau [23]. Once the tau aggregation cascade is initiated, the process begins to self-replicate. Unlike Aβ, proteopathic tau seeds are transferred from a "donor cell" to a "recipient cell" in a prion-like manner, where the seeds transform normal tau into aggregates (new seeds), driving the progression of neuronal degeneration and death [24–26]. The overall level of NFTs is closely related to degree of dementia [27,28].

Inhibition of tau aggregation is a suitable therapeutic strategy, and considerable progress has been made. There are currently two major approaches for addressing tau aggregation. One is to search for protein kinase inhibitors that inhibit tau hyperphosphorylation to prevent tau aggregation [29]. The other is to search for direct inhibitors of the tau aggregation process [30]. However, no matter which one is targeted alone, the tau cascade will not be easily broken. Therefore, the relationship between neuroinflammation and tau pathology has received increasing attention [31,32]. Not only that, systemic inflammation also provides a non-negligible contribution to AD [33]. Although inflammation may not be the initiating factor of AD, the vicious circle between it and neuronal lesions lead to increased neuronal degeneration [34,35]. Aggregated tau activates NLRP3-ASC inflammasome to aggravate neuroinflammation, and the occurrence of neuroinflammation not only increases abnormal tau hyperphosphorylation but also aggravates tau-seeded tau pathology [36–38]. Therefore, we aimed to develop anti-neuroinflammatory drug that can inhibit the tau aggregation process.

Natural products play a leading role in the discovery of drugs for the treatment of human diseases. Usnic acid (Fig. 1), a dibenzofuran derivative, is a high-level secondary metabolite in lichen [39]. Usnic acid has various biological characteristics owing to its special skeleton. Previous studies have shown that usnic acid has anticancer, antioxidant, anti-inflammatory, antiviral, and anti-pyretic activities [40]. Especially, the anti-inflammatory ability of usnic acid is potent. Different biological activities of usnic acid may be determined by its various fragments. The "triketone" moiety of usnic acid is an important fragment contributing to its bactericidal, anticancer, and cytotoxic activities [41], but it has little to do with the activities we need for the treatment of AD. Thus, we modified this (+) - moiety of usnic acid with the hope that the derivatives retain its anti-inflammatory activity and confer its ability to inhibit tau protein aggregation. Considering the poor water solubility of usnic acid, we used (+) - sodium usnate (Fig. 1) to improve its water solubility and bioavailability [42], and as a reference.

Herein, two series of compounds, compounds **1**–**25** as series A and **26**–**50** of series B, were synthesized and screened for AcPHF6 self-aggregation inhibitory activity by ThT assay. An optimal compound, **30**, was identified through CD spectrum and TEM image analyses. Noticeably, **30** also displayed an inhibitory activity against full-length tau aggregation. Further, **30** was initially evaluated for its anti-neuroinflammatory activity in BV-2 cells and for behavioral performance in a rat model of AD.

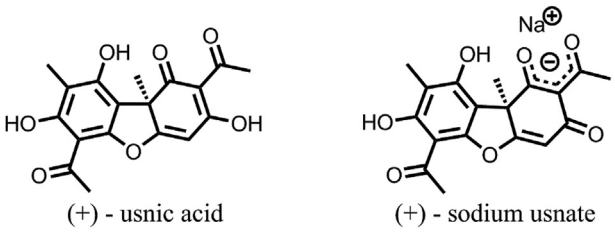

Fig. 1. Chemical structures of (+) - usnic acid and (+) - sodium usnate.

2. Results and discussion

2.1. Chemistry

Usnic acid derivatives were prepared according to previously published methods [43,44]. Enamine compounds **1, 4**–**25** were prepared through condensation of usnic acid with primary amines or amino acids (Scheme 1). Notably, the basicity of the amino group also affects the formation of an enamine bond with usnic acid. For example, 2-aminoquinoline and 2-aminothiazole cannot react with usnic acid under ordinary catalytic conditions, whereas 8-aminoquinoline can. In addition, pH (9.5–10) control is extremely important in the reaction of usnic acid with amino acids for preparing of **2** and **3**. The target compounds **26**–**50** were synthesized from the reaction of usnic acid with the corresponding hydrazines and hydrazides (Scheme 1). Interestingly, under the same conditions, aliphatic hydrazines and usnic acid did not react to form pyrazole rings. The structures of all target compounds were characterized by ^{1}H NMR, ^{13}C NMR, and HRMS.

2.2. Biological assays

2.2.1. ThT fluorescence assay

AcPHF6 (Ac-$_{306}$VQIVYK$_{311}$-NH$_2$) is a short peptide in the third repeat of the microtubule-binding region of tau protein. Studies have shown that AcPHF6 plays a dominant role in the initiation of tau aggregation [45]. As AcPHF6 forms a cross-β structure fiber spontaneously *in vitro*, it is a suitable model to study small-molecule inhibitors of tau aggregation [46]. Polyphenolic flavone myricetin and dye orange G (Fig. 2) are well-known inhibitors of AcPHF6 [47,48]. Aurones (Fig. 2), a subclass of the naturally occurring flavonoids, exhibited comparable inhibitory activity to myricetin [47]. And 5-nitro-a-cyanocarboxamide derivatives of caffeic acid (Fig. 2) showed a higher inhibitory activity (90% inhibition) at 50 μM [49]. In addition, peptides and macrocyclic peptides (Fig. 2) based on the structure of AcPHF6 also effectively reduced the aggregation process of AcPHF6 [50,51].

In the screening phase, we evaluated the ability of the target compounds to inhibit amyloid formation using ThT fluorescence assay. When ThT interacts with β-sheet-rich amyloid fibrils, its excitation and emission maxima are red-shifted to 440 and 490 nm, respectively [52]. In general, emission intensity at 490 nm reflects the amount of amyloid fiber. The kinetics of AcPHF6 aggregation (100 μM) in the absence of inhibitors was assessed in 50 mM phosphate buffer in the presence of ThT (20 μM). As reported previously [48], AcPHF6 aggregates rapidly at 25 °C and reaches a fluorescence maximum after an average time of 40 min (Fig. 3). On the basis of the above conditions, we tested the inhibitory ability of usnic acid derivatives at a concentration of 10 μM with myricetin as control. Excitingly, 38 of the 50 compounds exhibited inhibitory activity (Tables 1 and 2). Among them, compounds **18** and **30** were the most active compounds, with inhibition rates of 58% and 52%, respectively.

In series A, compounds **1**, **2**, and **3** were reported and used in antiviral and bactericidal applications. Same as sodium usnate, **1** did not exhibit inhibitory effect on tau aggregation. Interestingly, the introduction of different amino acids to usnic acid resulted in significant differences in activity, as evident for **2** and **3**. The tryptophan and carbonyl groups on both sides of compound **2** may constitute an important active group, which was similar to the NQTrp reported by *M. Frenkel-Pinter* et al. [53,54]. Addition of long chains (**4**) did not improve the inhibitory activity of sodium usnate. After the addition of poly-substituted phenols, hydroxyl

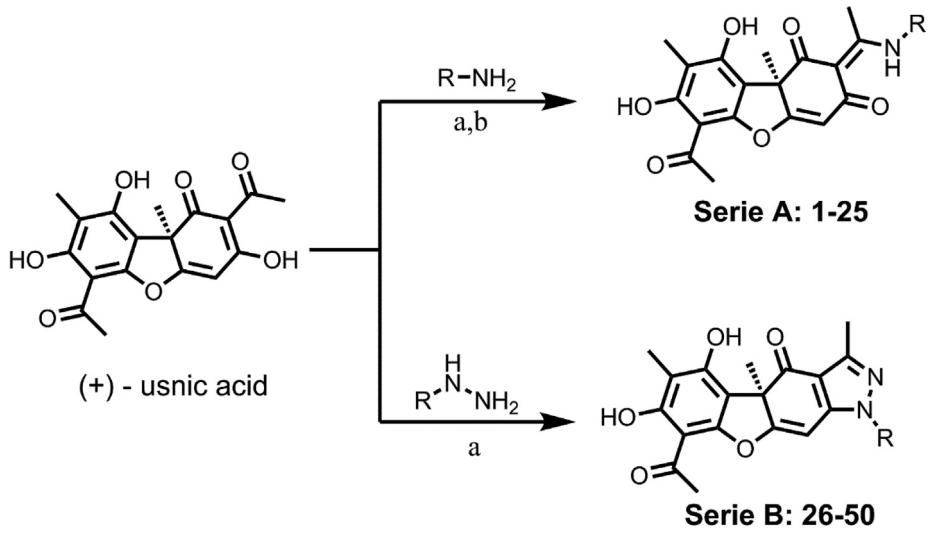

Scheme 1. Synthesis of compounds **1**–**50**. Reagents and conditions: (a) EtOH, 80 °C, 2–4 h. (b) EtOH/H_2O, KOH (pH~9.5), 80 °C, 4 h.

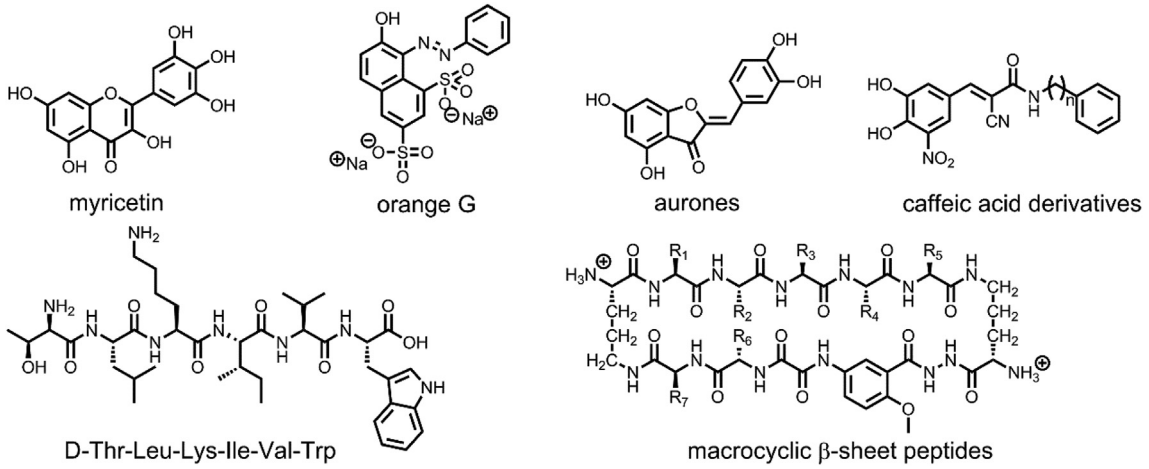

Fig. 2. Chemical structures of AcPHF6 aggregation inhibitors: myricetin; orange G; aurones; caffeic acid derivatives; pepetid D-TLKIVW and macrocyclic peptides.

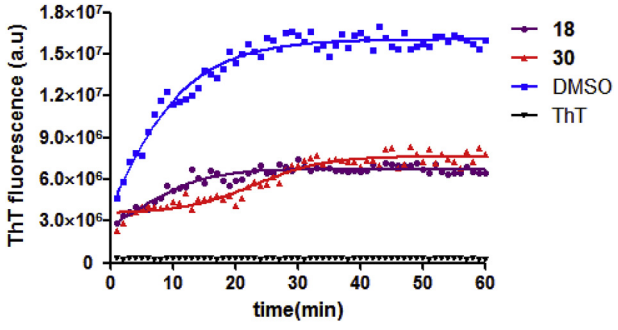

Fig. 3. Kinetics of 100 μM AcPHF6 aggregation in the absence (blue point) and presence of 10 μM **18** (purple point) and **30** (red point), as monitored by ThT fluorescence. (For interpretation of the references to colour in this figure legend, the reader is referred to the Web version of this article.)

substituents in the *ortho* position of enamine (**5**–**8**) show a certain inhibitory activity. However, when the hydroxyl group is in its *para* position (**9**–**11**), there is no activity regardless of the steric hindrance around the hydroxyl group. Compounds **12**–**16** showed that strong electron-donating and strong electron-withdrawing groups brought significant contribution to the activity observed, and that the position of the *N, N*-dimethyl group in *meta* (**16**) was less important than that in *para* (**15**), but the increase in steric hindrance (**14**) did not further increase the inhibitory activity. The addition of heterocycles indicated that small moieties, such as pyridine or pyrazine, as in **17**–**20**, were significantly better than the bulky moieties **21**–**25** in testing. In contrast to phenyl, pyridine as a substituent lead to the hydroxyl group in the para position of the enamine bond (**18**) exhibiting the best tau-inhibitory activity. Correspondingly, the replacement of the amino group at the same position (**19**) reduced the activity, showing the importance of the hydroxyl group.

In series B, the starting compound, **26**, had a moderate tau-inhibitory capacity, which may be related to its high planarity. Addition of fluorophenyl, tert-butylphenyl, methoxyphenyl, or benzonitrile, as in **27**–**28**, **29**, **34**–**35,** and **44**, seemed not to affect their activity, compared with that of **26**. However, different substituted benzoic acid groups (**30**–**32**) and 4-benzenesulfonamide (**37**) resulted in a good inhibitory activity. Compared with that of **31** and **32**, the tau-inhibitory activity of **30** was successively increased, suggesting that the position of the carboxyl group was more beneficial in the *para* position than that in

Table 1
Effect of compounds **1**–**25** on AcPHF6 self-aggregation.

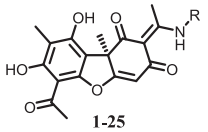

1-25

Compd.	R	Inhibition% (10 μM)[a]	Compd.	R	Inhibition% (10 μM)
1		n.a.[b]	**14**		48.2 ± 1.7
2	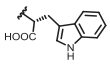	47.6 ± 16.4	**15**		48.1 ± 3.6
3		n.a.	**16**		11.3 ± 8.8
4	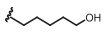	n.a.	**17**		48.0 ± 7.6
5		22.0 ± 12.0	**18**		58.3 ± 4.6
6		48.4 ± 12.2	**19**		46.4 ± 3.4
7		12.7 ± 9.7	**20**		44.2 ± 4.7
8		25.3 ± 20.1	**21**		n.a.
9		n.a.	**22**		n.a.
10		n.a.	**23**		39.2 ± 18.4
11		n.a.	**24**		27.6 ± 13.5
12		5.4 ± 2.0	**25**		29.8 ± 9.5
13		27.6 ± 13.4			
Myricetin		85.9 ± 1.3	Sodium Usnate		n.a.

[a] The inhibitory rates are shown as the mean ± SD from three separate experiments, each run in triplicate.
[b] n.a. means no activity.

the *meta* and *ortho* positions. However, replacing a carboxyl group with an ethyl ester group (**33**) greatly reduced tau-inhibitory activity, which was consistent with the result of replacing a sulfonamide group (**37**) and a methylsulfone group (**38**). The introduction of heterocycles was only moderately improved by pyridazine (**42**) and pyrazine (**43**), and most of the other heterocycles (**38**, **40**–**41**, and **45**–**47**) even showed decreased inhibitory activity compared to that of **26**. Notably, when a sulfo group was added between the pyrazole ring and the benzene ring, as in **48**–**50**, the compounds did not exhibit inhibitory activity regardless of the substituent on the phenyl ring, which may be attributed to the sulfo group blocking the conjugation and the planar structure.

Fig. 3 shows the aggregation kinetics of AcPHF6 in the presence of the optimal compounds **18** and **30**. Indeed, the spectral properties of ThT combined with fiber aggregates are influenced by a number of factors [52], such as the nature of the compound, composition of the medium, and protein-to-dye ratios. Therefore, to exclude false-positives that may be generated in ThT fluorescence assay, we further verified the activity of **18** and **30** using circular dichroism spectroscopy.

2.2.2. Circular dichroism (CD) spectroscopy

Based on the experimental conditions of the ThT assay, circular dichroism was used to further elucidate the degree of AcPHF6 aggregation inhibition by usnic acid derivatives **18** and **30** (Fig. 4). Owing to the morphological diversity of β-sheet-rich structures, we did not quantify the content of the secondary structure by CD spectrum [55]. The CD spectrum of AcPHF6 in the absence of an inhibitor (black line) showed a negative band at 221 nm and a positive band at 200 nm, which is a typical feature of the β-sheet structure [56]. A decrease in intensity was observed for the CD spectrum of AcPHF6 in the presence of **18** (blue line) and **30** (red line), suggesting that the abundance of β-sheet structures was lower. Unexpectedly, the activity of **30** was significantly higher than

Table 2
Effect of compounds **26**–**50** on AcPHF6 self-aggregation.

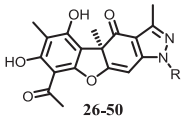

26-50

Compd.	R	Inhibition% (10 μM)	Compd.	R	Inhibition% (10 μM)
26		22.5 ± 9.4	**39**		29.8 ± 5.2
27		30.3 ± 5.1	**40**		17.1 ± 8.5
28		26.9 ± 9.0	**41**		7.7 ± 2.8
29		22.3 ± 10.4	**42**		40.9 ± 5.0
30		51.7 ± 3.6	**43**		38.0 ± 3.9
31		40.4 ± 6.1	**44**		20.1 ± 9.4
32		32.8 ± 4.2	**45**		12.2 ± 9.2
33		14.5 ± 4.8	**46**		n.a.
34		27.2 ± 3.2	**47**		9.3 ± 1.3
35		24.0 ± 1.5	**48**		n.a.
36		28.7 ± 9.8	**49**		n.a.
37		46.8 ± 1.1	**50**		n.a.
38		8.5 ± 7.7			
Myricetin		85.9 ± 1.3	**Sodium Usnate**		n.a.

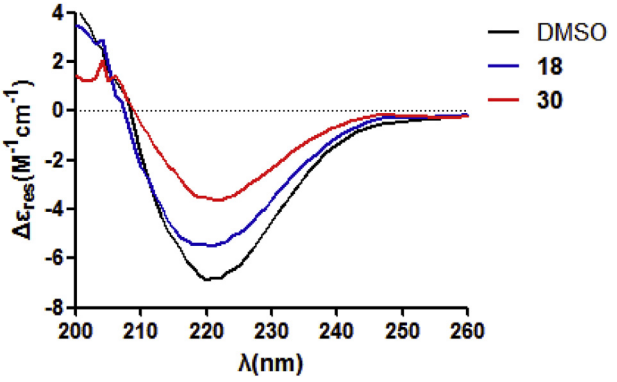

Fig. 4. CD spectra obtained after incubation of 100 μM AcPHF6 for 2 h at 25 °C in the absence (black) or presence of 10 μM of **18** (blue) and **30** (red). (For interpretation of the references to colour in this figure legend, the reader is referred to the Web version of this article.)

that of **18**, and this result was inconsistent with the ThT fluorescence result that the inhibitory activity of **18** was slightly higher than that of **30**.

In addition, the combination of compounds with amyloid fibers in the form of probes rather than inhibitors can also reduce the intensity of the CD spectrum [47]. Thus, we used transmission electron microscopy (TEM) to verify our findings.

2.2.3. Transmission electron microscopy

TEM allows visual observation of the aggregation pattern and progress of amyloid fibers [57]. We first observed the fiber morphology of AcPHF6 spontaneously accumulated in phosphate buffer for 2 h, as shown in Fig. 5A. The hexapeptide aggregated into a network of filament fibers. Although the addition of **18** (Fig. 5B) led to the fiberation process of AcPHF6, the long, twisted fiber structure obviously still existed. However, we found an encouraging result that, as shown in Figs. 5C, **30** exerted strong inhibitory activity against AcPHF6 aggregation, with almost no fibrillar material was observed in the field of view, and finally a dot-like structure (<5 nm) was formed.

Taken together, CD data and TEM results confirmed the inhibitory capacity of usnic acid derivatives **18** and **30**, with **30** as the most effective among the two derivatives. Therefore, we considered **30** the best aggregation inhibitor of AcPHF6 and used it for further

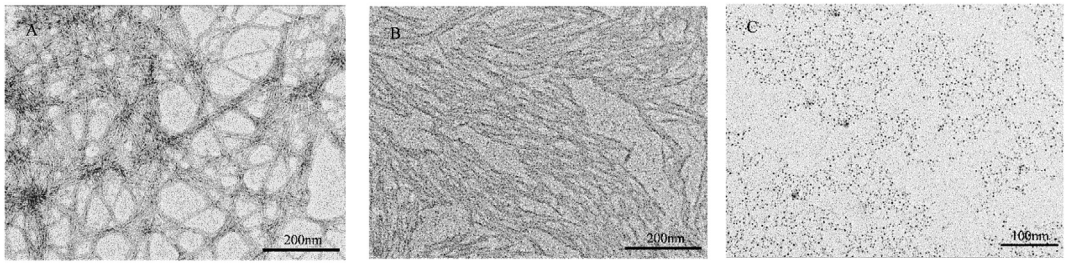

Fig. 5. TEM images of inhibition of AcPHF6 self-aggregation: (A) AcPHF6 (200 μM) alone; (B) AcPHF6 (200 μM) + **18** (20 μM) and (C) AcPHF6 (200 μM) + **30** (20 μM).

studies.

2.2.4. Full-length tau aggregation and inhibition studies

The adult human brain contains six major tau isoforms [19]. We used the most representative full-length 2N4R tau to verify the inhibitory ability of **30**. Indeed, owing to the lack of post-translational modifications, recombinant tau protein does not substantially undergo self-aggregation under physiological conditions. Addition of anionic cofactors, such as heparin and arachidonic acid, is a method that promotes the use of recombinant tau aggregation [58]. Here, we evaluated the effect of **30** (10 μM) on the tau aggregation process under heparin induction, which was monitored by ThT assay. Fig. 6 shows that treatment of full-length tau protein with **30** significantly slowed down the aggregation process and reduced the amount of formed aggregates (50% inhibition). Importantly, this result corresponded to the inhibition of AcPHF6 self-aggregation by **30**, confirming the potential of **30** as a tau anti-aggregation compound.

2.2.5. Neuro- and hepatotoxicity assessments

Considering the toxicity of usnic acid [59], we tested the cytotoxicity of its derivative, **30**, *in vitro* with the hope that its safe range would be acceptable. Human neuroblastoma SK-N-SH (SH-SY5Y) cells and human hepatocyte (LO2) cells are suitable models for detecting neurotoxicity and hepatotoxicity of compounds. First, SH-SY5Y cells were treated with **30** at concentrations of 10–40 μM for 24 h, and cell viability was assessed by the MTT test. Fig. 7A shows that **30** at 30 μM reduced the survival of SH-SY5Y cells. Similarly, LO2 cells were incubated with **30**, and as show in Figs. 7B, **30** exerted no significant hepatotoxicity even at high concentrations (up to 40 μM).

2.2.6. Inhibition of NO release studies

Excessive activation of microglia plays a crucial role in neuronal damage and death caused by neuroinflammation in AD [60]. Some studies revealed that tau pathology is prone to trigger activation of microglia [61]. Correspondingly, the inflammatory factors released by activated microglia can also aggravate tauopathies, either by inducing tau aggregation or hyperphosphorylation [32,36]. Therefore, inhibition of neuroinflammatory cytokine production is considered an effective strategy for the treatment of AD.

NO release is an important feature of microglial activation, and it may lead to an uncontrolled increase in neuroinflammation [62,63]. In a culture medium, NO is rapidly oxidized to nitrite, and nitrite (NO_2) concentration is an indicator of NO production, which can be detected by the Griess assay. Before this, we determined the cytotoxicity of **30** and sodium usnate against the viability of BV2 cells by using MTT assay, and the results showed that **30** at a concentration of 20 μM exerted no effect on BV2 cell viability (Fig. 8A), whereas sodium usnate at the same concentration exhibited acute cytotoxic effect (Fig. 8B). Thus, we investigated whether **30** exerts anti-inflammatory activity without affecting cell viability, with 10 μM sodium usnate as a control. As shown in Figs. 8C, **30** at a concentration of 10 μM retained the anti-inflammatory activity of sodium usnate and inhibited NO release rate by 41%.

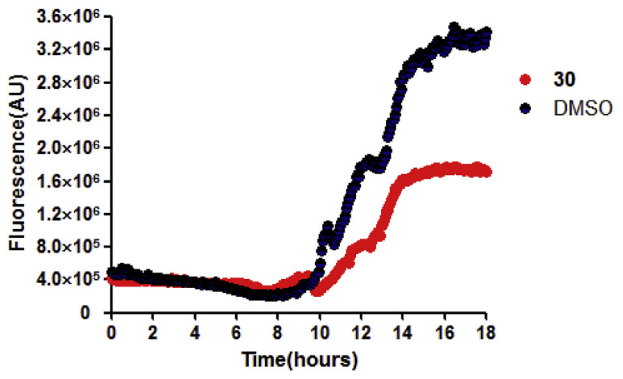

Fig. 6. Kinetics of **30** activity on heparin-induced full-length 2N4R tau aggregation, as monitored by ThT fluorescence.

*2.2.7. Compound **30** ameliorates learning and memory impairments in AD model rats*

Okadaic acid (OA)-induced memory impairment in rats is a suitable model for assessing the therapeutic efficiency of anti-AD agents *in vivo*. OA is a selective inhibitor of the serine/threonine phosphatases 2 (PP2A), and thereby induces tau hyperphosphorylation [64]. We injected OA to the ipsilateral hippocampus of rats to establish AD models after 7 days of intraperitoneal injection of **30** (at 5 and 10 mg/kg) or saline. The rats develop dementia after 3 days of OA injection into the brain. After OA injection was completed, the rats continued to be intraperitoneally administered **30** for 7 days, and the Morris water maze test was carried out to evaluate the cognition-improving effect of **30**.

During the experimental period, **30** exerted no acute toxicity symptoms, such as mortality or abnormal body weight change. Fig. 9A shows changes in body weight of rats injected intraperitoneally with **30** for 14 days. During the 5-day training, the average escape latency and search distance of each group of mice gradually decreased, but model rats usually spent more time and walked further distances to find the hidden platform. Fig. 9B shows the mean values of the escape latencies to the hidden platform at day 1–5. Compared with that on day 1 of training, the average escape time of model-operated rats on day 5 decreased from 50.0 to 41.8 s, whereas the average escape time of control-operated rats decreased from 37.2 to 12.5 s over the course of the same training days. Compared with the control group, the high-dose (10 mg/kg) **30**-treated group had a shorter escape latency than the low-dose (5 mg/kg) **30**-treated group, showing an average escape time from 45.9 to 18.5 s. At the same time, we also recorded the average

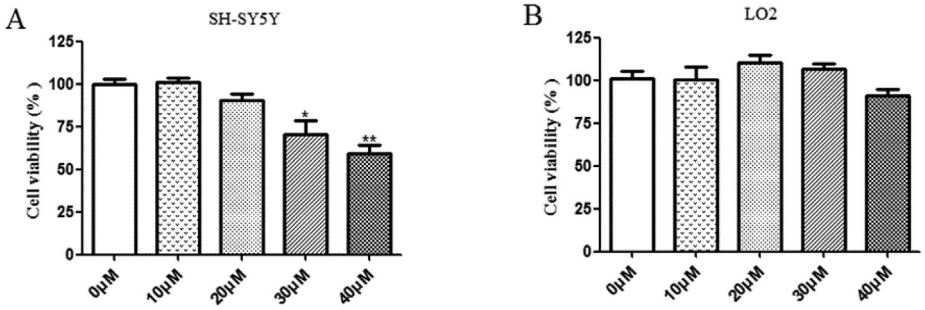

Fig. 7. (A) Viability of SH-SY5Y cells was determined by the MTT assay after 24 h of incubation with various concentrations of **30**. (B) Viability of LO2 cells was determined by the MTT assay after 24 h of incubation with various concentrations of **30**. The results are expressed as a percentage of control cells. Values are reported as the mean and SD of three independent experiments, each run in triplicate.

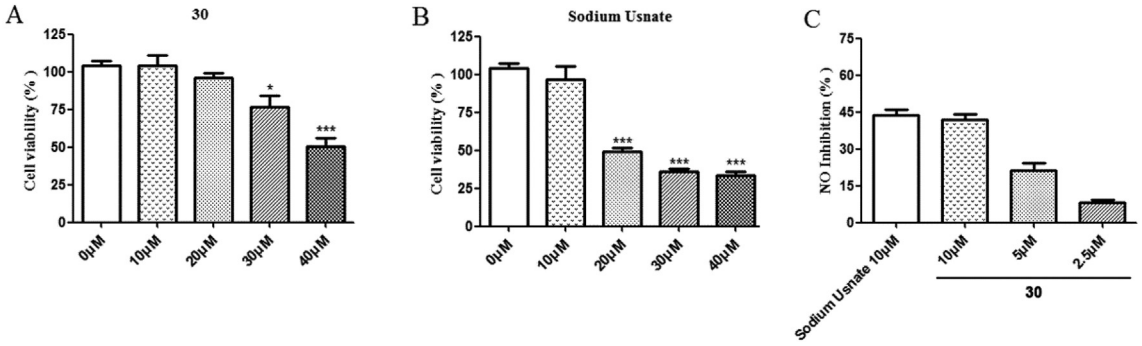

Fig. 8. Viability of BV2 cells was determined by the MTT assay after 24 h of incubation with various concentrations of **30** (A) and sodium usnate (B). The results are expressed as a percentage of control cells. (C) Effect of **30** on LPS-stimulated production of the inflammatory mediator NO in BV-2 cells, compared with that of sodium usnate. Griess assay was used to detect NO production. Results are expressed as percent of cells treated with LPS alone. All values are reported as the mean ± SD of three independent experiments, each run in triplicate.

swimming speed of each group of rats in the maze. There was no difference in the average swimming speed (Fig. 9C) between the groups, indicating that intake of **30** during the experiment did not affect the rats' normal physiology activity. Furthermore, in the probe trial on day 6, after the platform was removed, the time of rats staying in the target quadrant and the number of crossing the virtual platform (the original platform location) were significantly higher in the high-dose and control groups than in the model group (Fig. 9D and E). Representative trajectories of the rats in the Morris water maze during the spatial probe trial period (Fig. 9F) showed purposeful and regular search for hidden platforms in the treatment and control group rats, but showed random motion paths in model rats. These results further revealed that **30** administration led to a substantial improvement of the conventional reference spatial memory and cognitive abilities of rats.

3. Conclusion

In summary, two series of usnic acid derivatives were synthesized and tested for their tau-aggregation inhibitory activities. We used the tau-derived hexapeptide AcPHF6 model, a fragment that mainly promotes tau aggregation, to evaluate the activity of the derivatives. Among them, compounds **18** and **30** were the most prominent, with inhibitory activities of 58% and 52%, respectively. As the ThT fluorescence assay was affected by many factors, there might have been a certain degree of false positives in the results. Therefore, we used CD spectrum and TEM assays to determine whether **30** inhibits AcPHF6 self-polymerization, and TEM results showed that **30**, compared with the control, stopped the formation of AcPHF6 filaments and promoted the formation AcPHF6 dot structures. Encouragingly, **30** also exerted excellent inhibitory activity against the aggregation of full-length 2N4R tau protein. In addition, **30** at concentrations below 20 μM showed no apparent cytotoxicity to SH-SY5Y cells and mouse microglia BV2 cells, and it also showed low hepatotoxicity even at a high concentration of 40 μM. Moreover, **30** at 10 μM significantly reduced NO release by LPS-induced BV2 cells, indicating that it had excellent anti-neuroinflammatory activity. Most importantly, the results of the Morris water maze test showed that **30** enhanced the cognitive ability of OA-induced AD model rats. All these results highlighted **30** as a potential candidate for the development of anti-AD drugs.

4. Experimental section

4.1. Chemistry

All conventional reagents and solvents were purchased directly from commercial companies and without further purification. Reaction progress was monitored using analytical thin layer chromatography on precoated silica gel GF254 plates (Qingdao Haiyang Chemical Plant, Qingdao, China) and the spots were detected under UV light (254 nm). After post-treatment of the reaction, the product was separated by rapid purification preparative liquid chromatography (Biotage, Isolera One, Sweden). ^{1}H NMR and ^{13}C NMR spectra were measured with a Bruker ACF-500/600 spectrometer at 25 °C and referenced to TMS. The residual solvent line was designated as an internal standard and the chemical shift was reported in ppm (δ). High-resolution electrospray ionization (HRESI) mass spectra were carried out using an Agilent 6520B Q-TOF mass spectrometer (Agilent Technologies, Santa Clara, CA, USA).

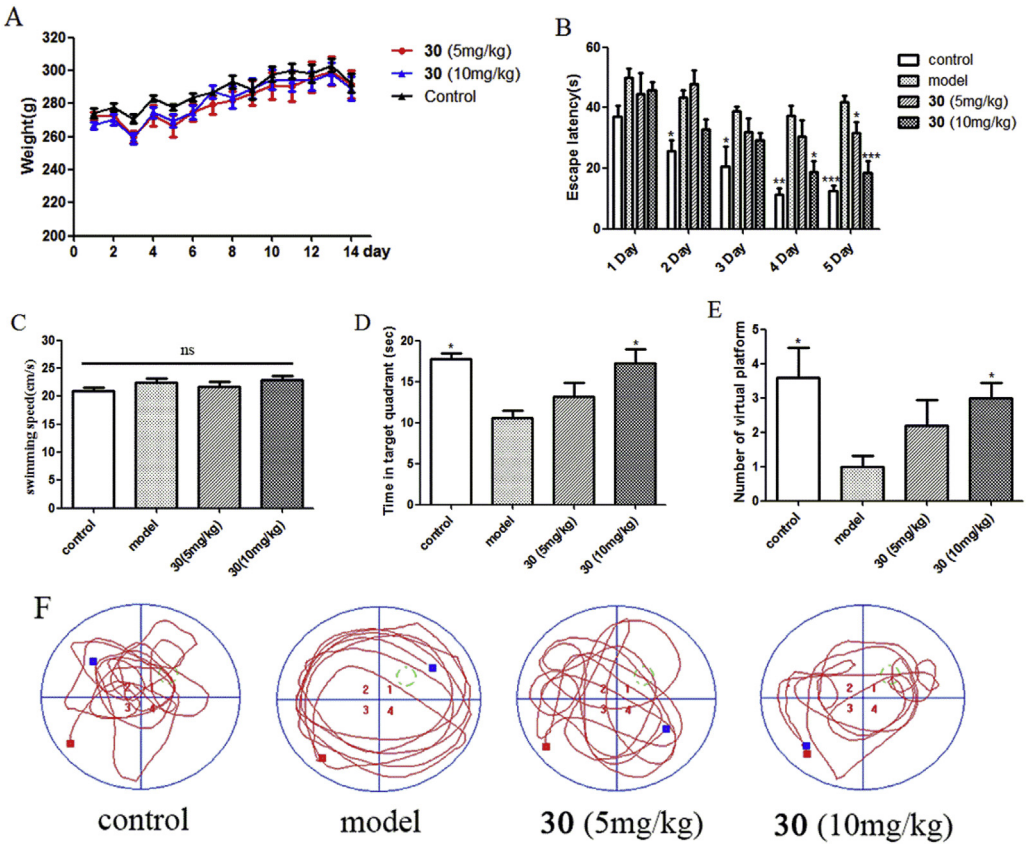

Fig. 9. Compound **30** attenuates OA-induced spatial learning and memory deficits in the training session of Morris water maze task. Data are presented as the mean ± SD (n = 8); statistical significance was evaluated by two-way ANOVA: $^{ns}p > 0.05$, $^{*}p < 0.05$, $^{**}p < 0.01$ and $^{***}p < 0.001$ compared with the model group. Error bars represent standard error of the mean. (A) Mean daily body weight profile of the control, 5 mg/kg **30**, and 10 mg/kg **30** groups during the 14-day drug administration period. (B) Escape latency time of each group was counted on day 1–5 during the training period. (C) Average swimming speed of rats in each group for 5 days. (D) Time spent in the virtual platform quadrant. (E) Number of virtual platform (the original platform location) crossings. (F) Representative tracks of rats in the Morris water maze during the spatial probe trial period. The blue solid coil represents the range of the maze, and the green dotted circle represents the position of the virtual platform. The red square point and the blue square point are the starting and ending positions of the rat, respectively. (For interpretation of the references to colour in this figure legend, the reader is referred to the Web version of this article.)

4.2. Synthesis

4.2.1. Preparation of compound ***1***

(+)-Usnic acid (1 equiv.) and concentrated ammonium hydroxide (10 equiv.) were added to absolute EtOH under nitrogen, and the reaction mixture was stirred at 80 °C for 2 h. After the reaction was completed, the solution was cooled to 25 °C and then acidified with 1 N hydrochloric acid. The mixed liquid was extracted twice with ethyl acetate. The combined extracts were then washed with H_2O and brine, and dried over anhydrous Na_2SO_4. After concentration under reduced pressure, the residue was quickly purified by using a silica gel column (PE/EtOAc).

*4.2.1.1. (R,E)-6-acetyl-2-(1-aminoethylidene)-7,9-dihydroxy-8,9b-dimethyldibenzo[b,d]furan-1,3(2H, 9bH)-dione (**1**).* Yield 72%, pale yellow powder. m.p. 255–256 °C. ^{1}H NMR (500 MHz, DMSO-d_6) δ 13.39 (s, 1H), 12.29 (s, 1H), 11.54 (bs, 1H), 9.80 (bs, 1H), 5.85 (s, 1H), 2.63 (s, 3H), 2.53 (s, 3H), 1.97 (s, 3H), 1.63 (s, 3H). ^{13}C NMR (126 MHz, DMSO-d_6) δ 200.8, 197.5, 188.4, 175.7, 172.9, 162.4, 157.6, 155.6, 106.2, 105.0, 102.5, 101.2, 100.8, 56.0, 31.5, 30.9, 24.4, 7.4. HRMS (ESI) *m/z* 342.0983 $[M - H]^-$ (calcd for 342.0986, $C_{18}H_{16}NO_6$).

4.2.2. General procedures for the preparation of ***2***–***3***

The reaction of (+) - usnic acid with amino acid was carried out as previously described [65], but with some modifications. Amino acid (3 equiv.) was suspended in aqueous ethanol (1:1, v/v) and KOH was added in portions while stirring until the amino acid was completely dissolved at 80 °C. (+) - Usnic acid was added to the clarified mixture and the pH was adjusted to 9.5 with KOH. The mixture was heated until the reaction was complete. Solution was cooled to room temperature and was acidified with 1 N hydrochloric acid. The mixed liquid was extracted twice with ethyl acetate, and the combined extracts were washed with H_2O and brine, dried over anhydrous Na_2SO_4. After concentration under reduced pressure, the residues were quickly purified by silica gel column (PE/EtOAc).

*4.2.2.1. (S)-2-(((E)-1-((R)-6-Acetyl-7,9-dihydroxy-8,9b-dimethyl-1,3-dioxo-1,9b-dihydrodibenzo[b,d]furan-2(3H)-ylidene)ethyl)amino)-3-(1H-indol-3-yl)propanoic acid (**2**).* Yield 80%, yellow powder. m.p. 150–152 °C. ^{1}H NMR (600 MHz, DMSO-d_6) δ 13.64 (bs, 1H), 13.41 (s, 1H), 13.37 (bs, 1H), 12.13 (s, 1H), 10.99 (s, 1H), 7.46 (dt, J = 8.2, 0.9 Hz, 1H), 7.33 (dt, J = 8.2, 0.9 Hz, 1H), 7.13 (d, J = 2.4 Hz, 1H), 7.05 (ddd, J = 8.0, 6.9, 1.1 Hz, 1H), 6.94 (ddd, J = 8.0, 6.9, 1.1 Hz, 1H), 5.84 (td, J = 7.8, 4.8 Hz, 1H), 5.05 (m, 1H), 3.30–3.40 (m, 2H), 2.64 (s, 3H), 2.37 (s, 3H), 1.97 (s, 3H), 1.62 (s, 3H). ^{13}C NMR (126 MHz, DMSO-d_6) δ 200.8, 197.4, 188.6, 174.3, 172.8, 171.1, 162.4, 157.5, 155.7, 136.0, 127.0, 124.4, 121.0, 118.5, 118.0, 111.3, 107.5, 106.2, 105.0, 102.3, 101.7, 100.8, 56.9, 56.2, 31.5, 30.9, 28.3, 18.5, 7.4. HRMS (ESI) *m/z* 529.1616 $[M - H]^-$ (calcd for 529.1612, $C_{29}H_{26}N_2O_8$).

*4.2.2.2. (S)-2-(((E)-1-((R)-6-Acetyl-7,9-dihydroxy-8,9b-dimethyl-1,3-dioxo-1,9b-dihydrodibenzo[b,d]furan-2(3H)-ylidene)ethyl) amino)-3-phenylpropanoic acid (**3**).* Yield 86%, pale yellow powder. m.p. 239–240 °C. ^{1}H NMR (600 MHz, DMSO-d_6) δ 13.72 (bs, 1H), 13.40 (s, 1H), 13.37 (bs, 1H), 12.10 (s, 1H), 7.27–7.19 (m, 5H), 5.88 (s, 1H), 5.09 (td, J = 7.6, 4.9 Hz, 1H), 3.28–3.14 (m, 2H), 2.64 (s, 3H), 2.38 (s, 3H), 1.97 (s, 3H), 1.64 (s, 3H). ^{13}C NMR (126 MHz, DMSO-d_6) δ 201.4, 198.2, 189.2, 175.1, 173.4, 171.2, 163.0, 158.1, 156.2, 135.9, 130.0, 128.9, 127.6, 106.8, 105.6, 102.9, 102.3, 101.4, 57.8, 56.9, 38.5, 32.1, 31.5, 19.0, 8.0. HRMS (ESI) *m/z* 490.1507 [M - H]$^-$ (calcd for 490.1511, $C_{27}H_{24}NO_8$).

*4.2.3. General procedures for the preparation of **4**–**25***

(+)-Usnic acid (1 equiv.) and primary ammonia compounds (1.1 equiv.) were added in absolute EtOH under nitrogen and the reaction mixture was stirred at 80 °C for 4 h. For the hydrochloride salt materials, they (1.1 equiv) were added to absolute ethanol, and an equivalent amount of pyridine (1.1 equiv) was added dropwise thereto and stirred at 80 °C under nitrogen. After 5 min, (+) - usnic acid was added and the reaction mixture was stirred for another 4 h. After reaction was complete, the reaction solution was cooled and concentrated under reduced pressure. The residues were quickly purified by silica gel column (PE/EtOAc).

*4.2.3.1. (R,E)-6-acetyl-7,9-dihydroxy-2-(1-((5-hydroxypentyl)amino) ethylidene)-8,9b-dimethyldibenzo[b,d]furan-1,3(2H,9bH)-dione. (**4**).* Yield 79%, pale yellow powder. m.p. 127–129 °C. ^{1}H NMR (500 MHz, DMSO-d_6) δ 13.39 (s, 1H), 13.05 (t, J = 5.3 Hz, 1H), 12.32 (s, 1H), 5.86 (s, 1H), 4.38 (t, J = 5.1 Hz, 1H), 3.54 (t, J = 6.7 Hz, 2H), 3.42 (q, J = 6.2 Hz, 2H), 2.64 (s, 3H), 2.59 (s, 3H), 1.97 (s, 3H), 1.65 (m, 5H), 1.53–1.44 (m, 2H), 1.43–1.37 (m, 2H). ^{13}C NMR (126 MHz, DMSO-d_6) δ 201.4, 197.7, 189.5, 175.3, 173.5, 163.0, 158.2, 156.2, 106.8, 105.6, 102.8, 102.0, 101.4, 60.9, 56.8, 44.0, 32.4, 32.2, 31.5, 28.6, 23.4, 18.6, 8.0. HRMS (ESI) *m/z* 428.1715 [M - H]$^-$ (calcd for 428.1730, $C_{23}H_{27}NO_7$).

*4.2.3.2. (R,E)-6-acetyl-2-(1-((5-chloro-2-hydroxyphenyl)amino)ethylidene)-7,9-dihydroxy-8,9b-dimethyldibenzo[b,d]furan-1,3(2H,9bH)-dione. (**5**).* Yield 89%, yellow powder. m.p. 154–155 °C. ^{1}H NMR (500 MHz, DMSO-d_6) δ 14.53 (bs, 1H), 13.40 (s, 1H), 12.02 (s, 1H), 10.62 (s, 1H), 7.47 (d, J = 3.5 Hz, 1H), 7.30 (dd, J = 8.5, 3.5 Hz, 1H), 7.03 (d, J = 8.5 Hz, 1H), 6.00 (s, 1H), 2.66 (s, 3H), 2.52 (s, 3H), 1.99 (s, 3H), 1.71 (s, 3H). ^{13}C NMR (126 MHz, DMSO-d_6) δ 201.4, 198.6, 190.0, 175.0, 174.2, 163.1, 158.0, 156.2, 151.2, 129.6, 127.1, 124.7, 122.9, 118.2, 107.0, 105.5, 103.0, 102.7, 101.5, 57.2, 32.1, 31.5, 20.8, 8.0. HRMS (ESI) *m/z* 468.0856 [M - H]$^-$ (calcd for 468.0852, $C_{27}H_{19}ClNO_7$).

*4.2.3.3. (R,E)-6-acetyl-2-(1-((4-chloro-2-hydroxyphenyl)amino)ethylidene)-7,9-dihydroxy-8,9b-dimethyldibenzo[b,d]furan-1,3(2H,9bH)-dione. (**6**).* Yield 84%, yellow powder. m.p. 147–149 °C. ^{1}H NMR (500 MHz, DMSO-d_6) δ 14.52 (bs, 1H), 13.40 (s, 1H), 12.03 (s, 1H), 10.87 (s, 1H), 7.36 (d, J = 8.5 Hz, 1H), 7.05 (d, J = 2.3 Hz, 1H), 6.98 (dd, J = 8.5, 2.3 Hz, 1H), 5.98 (s, 1H), 2.66 (s, 3H), 2.51 (s, 3H), 1.98 (s, 3H), 1.71 (s, 3H). ^{13}C NMR (126 MHz, DMSO-d_6) δ 201.4, 198.5, 190.0, 174.8, 174.1, 163.0, 158.0, 156.2, 153.0, 133.4, 128.7, 122.8, 119.7, 116.7, 107.0, 105.5, 103.0, 102.7, 101.4, 57.2, 32.1, 31.5, 20.8, 8.0. HRMS (ESI) *m/z* 468.0856 [M - H]$^-$ (calcd for 468.0857, $C_{27}H_{19}ClNO_7$).

*4.2.3.4. (R,E)-6-acetyl-7,9-dihydroxy-2-(1-((2-hydroxy-5-methylphenyl)amino)ethylidene)-8,9b-dimethyldibenzo[b,d]furan-1,3(2H,9bH)-dione. (**7**).* Yield 82%, yellow powder. m.p. 134–136 °C. ^{1}H NMR (500 MHz, DMSO-d_6) δ 14.50 (bs, 1H), 13.41 (s, 1H), 12.12 (s, 1H), 10.05 (s, 1H), 7.11 (d, J = 2.0 Hz, 1H), 7.06 (dd, J = 8.2, 2.0 Hz, 1H), 6.92 (d, J = 8.2 Hz, 1H), 5.98 (s, 1H), 2.66 (s, 3H), 2.51 (s, 3H), 2.24 (s, 3H), 1.99 (s, 3H), 1.71 (s, 3H). ^{13}C NMR (126 MHz, DMSO-d_6) δ 201.4, 198.4, 190.0, 174.7, 174.0, 163.0, 158.0, 156.2, 149.6, 130.4, 128.8, 127.4, 123.1, 116.8, 106.9, 105.6, 102.8, 102.8, 101.4, 57.1, 32.2, 31.5, 20.8, 20.4, 8.0. HRMS (ESI) *m/z* 448.1402 [M - H]$^-$ (calcd for 448.1399, $C_{25}H_{22}NO_7$).

*4.2.3.5. (R,E)-6-acetyl-7,9-dihydroxy-2-(1-((2-hydroxy-4-methylphenyl)amino)ethylidene)-8,9b-dimethyldibenzo[b,d]furan-1,3(2H,9bH)-dione. (**8**).* Yield 84%, yellow powder. m.p. 132–134 °C. ^{1}H NMR (500 MHz, DMSO-d_6) δ 14.47 (bs, 1H), 13.40 (s, 1H), 12.13 (s, 1H), 10.20 (s, 1H), 7.17 (d, J = 8.0 Hz, 1H), 6.84 (d, J = 1.8 Hz, 1H), 6.73 (dd, J = 8.3, 1.8 Hz, 1H), 5.97 (s, 1H), 2.66 (s, 3H), 2.51 (s, 3H), 2.28 (s, 3H), 1.98 (s, 3H), 1.71 (s, 3H). ^{13}C NMR (126 MHz, DMSO-d_6) δ 201.4, 198.3, 189.9, 174.6, 174.0, 163.0, 158.0, 156.2, 151.7, 139.7, 126.9, 121.0, 120.6, 117.4, 106.9, 105.6, 102.8, 102.8, 101.4, 57.1, 32.2, 31.5, 21.4, 20.8, 8.0. HRMS (ESI) *m/z* 448.1402 [M - H]$^-$ (calcd for 448.1402, $C_{25}H_{22}NO_7$).

*4.2.3.6. (R,E)-6-acetyl-7,9-dihydroxy-2-(1-((4-hydroxy-2,6-dimethylphenyl)amino)ethylidene)-8,9b-dimethyldibenzo[b,d]furan-1,3(2H,9bH)-dione. (**9**).* Yield 76%, pale brown powder. m.p. 283–285 °C. ^{1}H NMR (600 MHz, DMSO-d_6) δ 14.03 (bs, 1H), 13.42 (s, 1H), 12.16 (s, 1H), 9.63 (s, 1H), 6.62 (d, J = 5.9 Hz, 2H), 6.00 (s, 1H), 2.66 (s, 3H), 2.32 (s, 3H), 2.07 (s, 3H), 2.02 (s, 3H), 1.98 (s, 3H), 1.72 (s, 3H). ^{13}C NMR (126 MHz, DMSO-d_6) δ 201.5, 198.3, 190.0, 176.6, 174.1, 163.0, 158.0, 157.5, 156.2, 135.9, 135.6, 125.9, 115.5, 106.9, 105.6, 102.8, 102.4, 101.4, 57.0, 32.2, 31.6, 19.7, 18.3, 18.2, 8.0. HRMS (ESI) *m/z* 462.1558 [M - H]$^-$ (calcd for 462.1559, $C_{26}H_{24}NO_7$).

*4.2.3.7. (R,E)-6-acetyl-7,9-dihydroxy-2-(1-((4-hydroxy-5-isopropyl-2-methylphenyl)amino)ethylidene)-8,9b-dimethyldibenzo[b,d]furan-1,3(2H,9bH)-dione. (**10**).* Yield 73%, yellow powder. m.p. 129–131 °C. ^{1}H NMR (500 MHz, DMSO-d_6) δ 14.41 (bs, 1H), 13.40 (s, 1H), 12.17 (s, 1H), 9.62 (s, 1H), 7.03 (s, 1H), 6.76 (s, 1H), 5.96 (s, 1H), 3.18 (hept, J = 7.0 Hz, 1H), 2.65 (s, 3H), 2.44 (s, 3H), 2.09 (s, 3H), 1.98 (s, 3H), 1.71 (s, 3H), 1.15 (dd, J = 7.0, 2.0 Hz, 6H). ^{13}C NMR (126 MHz, DMSO-d_6) δ 201.4, 198.2, 190.0, 175.2, 174.0, 163.0, 158.1, 156.2, 154.7, 133.7, 131.6, 126.4, 124.6, 117.3, 106.9, 105.6, 102.7, 102.6, 101.4, 57.1, 32.2, 31.5, 26.6, 22.9, 20.6, 17.6, 8.0. HRMS (ESI) *m/z* 490.1871 [M - H]$^-$ (calcd for 490.1871, $C_{28}H_{28}NO_7$).

*4.2.3.8. (R,E)-6-acetyl-2-(1-((3,5-di-tert-butyl-4-hydroxyphenyl) amino)ethylidene)-7,9-dihydroxy-8,9b-dimethyldibenzo[b,d]furan-1,3(2H,9bH)-dione. (**11**).* Yield 61%, yellow powder. m.p. 194–196 °C. ^{1}H NMR (600 MHz, DMSO-d_6) δ 14.62 (bs, 1H), 13.42 (s, 1H), 12.18 (s, 1H), 7.39 (s, 1H), 7.04 (s, 2H), 5.97 (s, 1H), 2.66 (s, 3H), 2.52 (s, 3H), 1.98 (s, 3H), 1.70 (s, 3H), 1.39 (s, 18H). ^{13}C NMR (151 MHz, DMSO-d_6) δ 200.8, 197.7, 189.4, 173.7, 173.3, 162.5, 157.4, 155.6, 153.5, 140.4, 127.5, 121.8, 106.3, 105.0, 102.1, 102.0, 100.8, 56.5, 34.7, 31.6, 31.0, 30.0, 20.3, 7.4. HRMS (ESI) *m/z* 546.2497 [M - H]$^-$ (calcd for 546.2500, $C_{32}H_{36}NO_7$).

4.2.3.9. (R,E)-6-acetyl-7,9-dihydroxy-8,9b-dimethyl-2-(1-((3,4,5-trimethoxyphenyl)amino)ethylidene)dibenzo[b,d]furan-1,3(2H,9bH)-dione. Yield 90%, yellow powder. (**12**). m.p. 210–212 °C. ^{1}H NMR (500 MHz, DMSO-d_6) δ 14.68 (bs, 1H), 13.39 (s, 1H), 12.03 (s, 1H), 6.76 (s, 2H), 5.98 (s, 1H), 3.81 (s, 6H), 3.70 (s, 3H), 2.65 (s, 3H), 2.58 (s, 3H), 1.98 (s, 3H), 1.71 (s, 3H). ^{13}C NMR (126 MHz, DMSO-d_6) δ 201.4, 198.6, 190.0, 174.8, 174.1, 163.1, 158.0, 156.2, 153.8, 137.5, 131.8, 107.0, 105.4, 104.1, 102.7, 102.7, 101.4, 60.6, 57.2, 56.7, 32.2, 31.5, 21.0, 8.0. HRMS (ESI) *m/z* 508.1613 [M - H]$^-$ (calcd for 508.1616, $C_{27}H_{26}NO_9$).

4.2.3.10. (R,E)-4-((1-(6-acetyl-7,9-dihydroxy-8,9b-dimethyl-1,3-dioxo-3,9b-dihydrodibenzo[b,d]furan-2(1H)-ylidene)ethyl)amino)-2-

*hydroxybenzoic acid. (**13**).* Yield 54%, pale yellow powder. m.p. 196–197 °C. ^{1}H NMR (600 MHz, DMSO-d_6) δ 14.74 (bs, 1H), 13.42 (s, 1H), 12.06 (s, 1H), 9.95 (s, 1H), 7.31 (m, 1H), 6.92–6.77 (m, 2H), 6.74 (s, 1H), 6.00 (s, 1H), 2.66 (s, 3H), 2.54 (s, 3H), 1.98 (s, 3H), 1.71 (s, 3H). ^{13}C NMR (151 MHz, DMSO-d_6) δ 200.7, 197.8, 189.4, 173.6, 173.4, 162.3, 158.0, 157.2, 155.4, 136.4, 130.2, 115.9, 115.0, 112.2, 106.2, 104.8, 102.0, 102.0, 100.7, 56.5, 31.4, 30.8, 20.2, 7.3. HRMS (ESI) *m/z* 478.1144 [M - H]$^-$ (calcd for 478.1160, $C_{25}H_{20}NO_9$).

*4.2.3.11. (R,E)-6-acetyl-7,9-dihydroxy-8,9b-dimethyl-2-(1-((4-(4-methylpiperazin-1-yl)phenyl)amino)ethylidene)dibenzo[b,d]furan-1,3(2H,9bH)-dione. (**14**).* Yield 87%, yellow powder. m.p. 216–217 °C. ^{1}H NMR (500 MHz, DMSO-d_6) δ 14.62 (bs, 1H), 13.41 (s, 1H), 12.14 (s, 1H), 7.22 (d, J = 9.0 Hz, 2H), 7.03 (d, J = 9.0 Hz, 2H), 5.98 (s, 1H), 3.21 (t, J = 5.1 Hz, 4H), 2.66 (s, 3H), 2.54 (s, 3H), 2.47 (t, J = 5.1 Hz, 4H), 2.24 (s, 3H), 1.99 (s, 3H), 1.71 (s, 3H). ^{13}C NMR (126 MHz, DMSO-d_6) δ 201.4, 198.3, 189.9, 174.1, 174.0, 163.0, 158.0, 156.2, 150.9, 126.6, 126.6, 115.8, 106.9, 105.6, 102.8, 102.7, 101.4, 57.1, 54.9, 48.0, 46.2, 32.2, 31.5, 20.8, 8.0. HRMS (ESI) *m/z* 516.2140 [M - H]$^-$ (calcd for 516.2144, $C_{29}H_{30}N_3O_6$).

*4.2.3.12. (R,E)-6-acetyl-2-(1-((4-(dimethylamino)phenyl)amino)ethylidene)-7,9-dihydroxy-8,9b-dimethyldibenzo[b,d]furan-1,3(2H,9bH)-dione. (**15**).* Yield 71%, yellow powder. m.p. 220–221 °C. ^{1}H NMR (500 MHz, DMSO-d_6) δ 14.59 (bs, 1H), 13.41 (s, 1H), 12.18 (s, 1H), 7.19 (d, J = 9.0 Hz, 2H), 6.79 (d, J = 9.0 Hz, 2H), 5.98 (s, 1H), 2.95 (s, 6H), 2.66 (s, 3H), 2.54 (s, 3H), 1.99 (s, 3H), 1.71 (s, 3H). ^{13}C NMR (126 MHz, DMSO-d_6) δ 201.4, 198.2, 189.9, 174.0, 173.9, 163.0, 158.1, 156.2, 150.3, 126.5, 124.3, 112.8, 106.9, 105.6, 102.8, 102.7, 101.4, 57.1, 40.5, 32.2, 31.5, 20.8, 8.0. HRMS (ESI) *m/z* 461.1718 [M - H]$^-$ (calcd for 461.1723, $C_{26}H_{25}N_2O_6$).

*4.2.3.13. (R,E)-6-acetyl-2-(1-((3-(dimethylamino)phenyl)amino)ethylidene)-7,9-dihydroxy-8,9b-dimethyldibenzo[b,d]furan-1,3(2H,9bH)-dione. (**16**).* Yield 74%, yellow powder. m.p. 198–199 °C. ^{1}H NMR (500 MHz, DMSO-d_6) δ 14.72 (bs, 1H), 13.41 (s, 1H), 12.09 (s, 1H), 7.29 (t, J = 8.1 Hz, 1H), 6.76 (dd, J = 8.5, 2.5 Hz, 1H), 6.65 (d, J = 2.3 Hz, 1H), 6.61 (dd, J = 7.6, 1.8 Hz, 1H), 5.99 (s, 1H), 2.93 (s, 6H), 2.66 (s, 3H), 2.56 (s, 3H), 1.99 (s, 3H), 1.71 (s, 3H). ^{13}C NMR (126 MHz, DMSO-d_6) δ 201.4, 198.5, 190.0, 174.5, 174.1, 163.1, 158.0, 156.2, 151.7, 136.9, 130.4, 113.0, 112.3, 109.3, 107.0, 105.5, 102.7, 102.7, 101.5, 57.2, 40.4, 32.2, 31.5, 20.9, 8.0. HRMS (ESI) *m/z* 461.1718 [M - H]$^-$ (calcd for 461.1719, $C_{26}H_{25}N_2O_6$).

*4.2.3.14. (R,E)-6-acetyl-7,9-dihydroxy-2-(1-((3-hydroxypyridin-2-yl)amino)ethylidene)-8,9b-dimethyldibenzo[b,d]furan-1,3(2H,9bH)-dione. (**17**).* Yield 58%, yellow powder. m.p. 229–231 °C. ^{1}H NMR (500 MHz, DMSO-d_6) δ 15.05 (bs, 1H), 13.39 (s, 1H), 11.89 (s, 1H), 10.99 (s, 1H), 7.99 (m, 1H), 7.41 (m, 1H), 7.27 (m, 1H), 5.99 (s, 1H), 2.85 (s, 3H), 2.66 (s, 3H), 1.99 (s, 3H), 1.72 (s, 3H). ^{13}C NMR (126 MHz, DMSO-d_6) δ 201.4, 199.1, 189.9, 174.0, 173.5, 163.0, 157.9, 156.2, 147.0, 139.4, 138.9, 124.3, 124.3, 107.0, 105.6, 104.1, 102.8, 101.5, 57.4, 31.9, 31.5, 21.3, 8.0. HRMS (ESI) *m/z* 435.1198 [M - H]$^-$ (calcd for 435.1199, $C_{23}H_{20}N_2O_7$).

*4.2.3.15. (R,E)-6-acetyl-7,9-dihydroxy-2-(1-((5-hydroxypyridin-2-yl)amino)ethylidene)-8,9b-dimethyldibenzo[b,d]furan-1,3(2H,9bH)-dione. (**18**).* Yield 63%, brown powder. m.p. 233–235 °C. ^{1}H NMR (600 MHz, DMSO-d_6) δ 14.90 (bs, 1H), 13.41 (s, 1H), 11.96 (s, 1H), 10.40 (s, 1H), 8.08 (d, J = 2.6 Hz), 7.45–7.27 (m, 2H), 6.00 (s, 1H), 2.65 (d, 6H), 1.99 (s, 3H), 1.71 (s, 3H). ^{13}C NMR (151 MHz, DMSO-d_6) δ 200.9, 198.3, 189.4, 173.6, 172.9, 162.5, 157.3, 155.6, 153.2, 140.6, 136.5, 124.6, 120.5, 106.4, 104.9, 102.4, 102.2, 100.9, 56.7, 31.4, 31.0, 20.4, 7.4. HRMS (ESI) *m/z* 435.1198 [M - H]$^-$ (calcd for 435.1199, $C_{23}H_{20}N_2O_7$).

*4.2.3.16. (R,E)-6-acetyl-2-(1-((5-aminopyridin-2-yl)amino)ethylidene)-7,9-dihydroxy-8,9b-dimethyldibenzo[b,d]furan-1,3(2H,9bH)-dione. (**19**).* Yield 59%, yellow powder. m.p. 242–244 °C. ^{1}H NMR (600 MHz, DMSO-d_6) δ 14.43 (bs, 1H), 13.41 (s, 1H), 12.10 (s, 1H), 7.92 (d, J = 2.8 Hz, 1H), 7.41 (dd, J = 8.8, 2.8 Hz, 1H), 6.52 (d, J = 8.7 Hz, 1H), 6.33 (s, 2H), 5.96 (s, 1H), 2.65 (s, 3H), 2.51 (s, 3H), 1.97 (s, 3H), 1.69 (s, 3H). ^{13}C NMR (151 MHz, DMSO-d_6) δ 200.8, 197.8, 189.3, 174.2, 173.4, 162.5, 159.1, 157.4, 155.6, 144.5, 134.5, 121.4, 107.7, 106.3, 104.9, 102.2, 102.1, 100.8, 56.5, 31.6, 31.0, 20.1, 7.4. HRMS (ESI) *m/z* 434.1358 [M - H]$^-$ (calcd for 434.1360, $C_{23}H_{21}N_3O_6$).

*4.2.3.17. (R,E)-6-acetyl-2-(1-((5-aminopyrazin-2-yl)amino)ethylidene)-7,9-dihydroxy-8,9b-dimethyldibenzo[b,d]furan-1,3(2H,9bH)-dione. (**20**).* Yield 62%, brown powder. m.p. 127–128 °C. ^{1}H NMR (600 MHz, DMSO-d_6) δ 14.76 (bs, 1H), 13.41 (s, 1H), 11.96 (s, 1H), 8.09 (d, J = 1.3 Hz, 1H), 7.80 (d, J = 1.4 Hz, 1H), 6.84 (s, 2H), 6.00 (s, 1H), 2.66 (s, 3H), 2.62 (s, 3H), 1.98 (s, 3H), 1.71 (s, 3H). ^{13}C NMR (151 MHz, DMSO-d_6) δ 200.9, 198.2, 189.3, 173.5, 173.1, 162.4, 157.3, 155.6, 155.0, 138.4, 134.5, 130.0, 106.4, 104.9, 102.5, 102.2, 100.8, 56.7, 31.4, 31.0, 20.4, 7.4. HRMS (ESI) *m/z* 435.1310 [M - H]$^-$ (calcd for 435.1313, $C_{22}H_{20}N_4O_6$).

*4.2.3.18. (R,E)-6-acetyl-7,9-dihydroxy-8,9b-dimethyl-2-(1-((1-methyl-1H-benzo[d]imidazol-5-yl)amino)ethylidene)dibenzo[b,d]furan-1,3(2H,9bH)-dione. (**21**).* Yield 78%, pale yellow powder. m.p. 246–247 °C. ^{1}H NMR (500 MHz, DMSO-d_6) δ 14.82 (bs, 1H), 13.41 (s, 1H), 12.11 (s, 1H), 8.31 (s, 1H), 7.86–7.60 (m, 2H), 7.28 (dd, J = 8.5, 2.0 Hz, 1H), 5.99 (s, 1H), 3.89 (s, 3H), 2.66 (s, 3H), 2.55 (s, 3H), 1.99 (s, 3H), 1.73 (s, 3H). ^{13}C NMR (126 MHz, DMSO-d_6) δ 201.4, 198.5, 190.0, 174.7, 174.1, 163.1, 158.0, 156.2, 146.9, 144.0, 134.6, 130.2, 120.6, 117.0, 111.6, 107.0, 105.6, 102.8, 102.7, 101.4, 57.2, 32.2, 31.5, 31.4, 20.8, 8.0. HRMS (ESI) *m/z* 472.1554 [M - H]$^-$ (calcd for 472.1537, $C_{26}H_{23}N_3O_6$).

*4.2.3.19. (R,E)-6-acetyl-7,9-dihydroxy-8,9b-dimethyl-2-(1-(quinolin-8-ylamino)ethylidene)dibenzo[b,d]furan-1,3(2H,9bH)-dione. (**22**).* Yield 87%, brown powder. m.p. 121–123 °C. ^{1}H NMR (500 MHz, DMSO-d_6) δ 15.41 (bs, 1H), 13.41 (s, 1H), 12.05 (s, 1H), 9.00 (dd, J = 4.2, 1.7 Hz, 1H), 8.51 (dd, J = 8.4, 1.7 Hz, 1H), 8.04 (dd, J = 8.2, 1.2 Hz, 1H), 7.92 (d, J = 7.4 Hz, 1H), 7.78–7.54 (m, 2H), 6.03 (s, 1H), 2.67 (s, 3H), 2.64 (s, 3H), 1.99 (s, 3H), 1.75 (s, 3H). ^{13}C NMR (126 MHz, DMSO-d_6) δ 201.4, 198.7, 190.0, 174.1, 174.1, 163.1, 158.0, 156.2, 151.6, 142.2, 137.2, 133.1, 129.1, 128.6, 126.7, 126.4, 123.2, 107.0, 105.6, 103.6, 102.8, 101.5, 57.3, 32.1, 31.5, 21.6, 8.0. HRMS (ESI) *m/z* 469.1405 [M - H]$^-$ (calcd for 469.1427, $C_{27}H_{22}N_2O_6$).

*4.2.3.20. (R,E)-2-(1-((1H-indol-5-yl)amino)ethylidene)-6-acetyl-7,9-dihydroxy-8,9b-dimethyldibenzo[b,d]furan-1,3(2H,9bH)-dione. (**23**).* Yield 66%, yellow powder. m.p. 260–261 °C. ^{1}H NMR (500 MHz, DMSO-d_6) δ 14.76 (bs, 1H), 13.41 (s, 1H), 12.18 (s, 1H), 11.37 (bs, 1H), 7.61–7.39 (m, 3H), 7.06 (dd, J = 8.6, 2.1 Hz, 1H), 6.50 (d, 1H), 6.00 (s, 1H), 2.67 (s, 3H), 2.56 (s, 3H), 1.99 (s, 3H), 1.73 (s, 3H). ^{13}C NMR (126 MHz, DMSO-d_6) δ 201.4, 198.3, 190.0, 174.5, 174.0, 163.0, 158.1, 156.2, 135.5, 128.3, 127.9, 127.7, 119.0, 117.4, 112.7, 106.9, 105.6, 102.8, 102.6, 102.1, 101.4, 57.1, 32.2, 31.5, 20.9, 8.0. HRMS (ESI) *m/z* 457.1405 [M - H]$^-$ (calcd for 457.1418, $C_{26}H_{22}N_2O_6$).

*4.2.3.21. (R,E)-6-acetyl-7,9-dihydroxy-8,9b-dimethyl-2-(1-((1-methyl-1H-indol-5-yl)amino)ethylidene)dibenzo[b,d]furan-1,3(2H,9bH)-dione. (**24**).* Yield 76%, yellow powder. m.p. 228–230 °C. ^{1}H NMR (500 MHz, DMSO-d_6) δ 14.77 (bs, 1H), 13.41 (s, 1H), 12.17 (s, 1H), 7.61–7.46 (m, 2H), 7.46 (d, J = 3.1 Hz, 1H), 7.13 (dd, J = 8.7, 2.0 Hz, 1H), 6.50 (d, J = 3.1 Hz, 1H), 5.99 (s, 1H), 3.84 (s, 3H), 2.67 (s, 3H), 2.55 (s, 3H), 1.99 (s, 3H), 1.73 (s, 3H). ^{13}C NMR (126 MHz, DMSO-d_6) δ 201.4, 198.4, 190.0, 174.5, 174.0, 163.1, 158.1, 156.2, 136.0, 132.1, 128.6, 127.8, 119.1, 117.7, 111.1, 106.9, 105.6, 102.8, 102.7, 101.5,

101.4, 57.1, 33.2, 32.2, 31.5, 20.9, 8.0. HRMS (ESI) *m/z* 471.1562 [M - H]$^-$ (calcd for 471.1580, $C_{27}H_{24}N_2O_6$).

*4.2.3.22. (R,E)-6-acetyl-2-(1-(benzo[d]thiazol-5-ylamino)ethylidene)-7,9-dihydroxy-8,9b-dimethyldibenzo[b,d]furan-1,3(2H,9bH)-dione. (**25**).* Yield 83%, pale yellow powder. m.p. 192–193 °C. ^{1}H NMR (600 MHz, DMSO-d_6) δ 14.93 (bs, 1H), 13.43 (s, 1H), 12.04 (s, 1H), 9.53 (s, 1H), 8.33 (d, J = 8.4 Hz, 1H), 8.19 (d, J = 2.0 Hz, 1H), 7.54 (dd, J = 8.5, 2.1 Hz, 1H), 6.04 (s, 1H), 2.67 (s, 3H), 2.59 (s, 3H), 2.00 (s, 3H), 1.74 (s, 3H). ^{13}C NMR (126 MHz, DMSO-d_6) δ 201.5, 198.7, 190.1, 174.8, 174.2, 163.1, 159.1, 158.0, 156.2, 153.9, 134.6, 133.9, 124.0, 123.8, 120.7, 107.0, 105.5, 103.0, 102.8, 101.5, 57.3, 32.1, 31.6, 21.0, 8.0. HRMS (ESI) *m/z* 475.0969 [M - H]$^-$ (calcd for 475.0976, $C_{25}H_{20}N_2O_6S$).

*4.2.4. General procedures for the preparation of **26**–**50***

(+)-Usnic acid (1 equiv.) and hydrazines/hydrazides (1.1 equiv.) were added in absolute EtOH under nitrogen and the reaction mixture was stirred at 80 °C for 2 h. For the hydrazines/hydrazides hydrochloride salt materials, they (1.1 equiv) were added to absolute ethanol, and an equivalent amount of pyridine (1.1 equiv) was added dropwise thereto and stirred at 80 °C under nitrogen. After 5 min, (+) - usnic acid was added and the reaction mixture was stirred for another 2 h. After reaction was complete, the reaction solution was cooled and concentrated under reduced pressure. The residues were quickly purified by silica gel column (PE/EtOAc).

*4.2.4.1. (R)-8-acetyl-5,7-dihydroxy-3,4a,6-trimethyl-1,4a-dihydro-4H-benzofuro[3,2-f]indazol-4-one. (**26**).* Yield 52%, yellow powder. m.p. 217–218 °C. ^{1}H NMR (500 MHz, DMSO-d_6) δ 13.67 (bs, 1H), 13.35 (s, 1H), 10.26 (s, 1H), 6.04 (s, 1H), 2.71 (s, 3H), 2.53 (s, 3H), 2.02 (s, 3H), 1.66 (s, 3H). ^{13}C NMR (126 MHz, DMSO-d_6) δ 201.6, 182.4, 180.4, 162.7, 156.6, 156.5, 156.4, 142.7, 111.4, 107.4, 106.5, 105.6, 102.1, 45.3, 33.6, 31.5, 10.8, 8.0. HRMS (ESI) *m/z* 339.0986 [M - H]$^-$ (calcd for 339.0989, $C_{18}H_{16}N_2O_5$).

*4.2.4.2. (R)-8-acetyl-1-(3-fluorophenyl)-5,7-dihydroxy-3,4a,6-trimethyl-1,4a-dihydro-4H-benzofuro[3,2-f]indazol-4-one. (**27**).* Yield 80%, orange powder. m.p. 176–177 °C. ^{1}H NMR (500 MHz, DMSO-d_6) δ 13.33 (s, 1H), 11.14 (s, 1H), 7.76–7.38 (m, 4H), 6.64 (s, 1H), 2.63 (s, 3H), 2.48 (s, 3H), 1.97 (s, 3H), 1.75 (s, 3H). ^{13}C NMR (126 MHz, DMSO-d_6) δ 201.4, 196.7, 172.9, 163.6, 163.0–161.7, 157.2, 156.8, 151.0, 149.3, 139.4–139.3, 132.0–131.9, 120.4–120.4, 116.0–115.9, 111.9–111.7, 110.8, 106.9, 104.8, 101.7, 90.5, 60.3, 31.5, 30.6, 13.5, 7.9. HRMS (ESI) *m/z* 433.1205 [M - H]$^-$ (calcd for 433.1211, $C_{24}H_{19}FN_2O_5$).

*4.2.4.3. (R)-8-acetyl-1-(4-fluorophenyl)-5,7-dihydroxy-3,4a,6-trimethyl-1,4a-dihydro-4H-benzofuro[3,2-f]indazol-4-one. (**28**).* Yield 48%, yellow powder. m.p. 218–219 °C. ^{1}H NMR (500 MHz, DMSO-d_6) δ 13.35 (s, 1H), 11.20 (s, 1H), 7.81–7.60 (m, 2H), 7.58–7.34 (m, 2H), 6.54 (s, 1H), 2.62 (s, 3H), 2.48 (s, 3H), 1.98 (s, 3H), 1.75 (s, 3H). ^{13}C NMR (126 MHz, DMSO-d_6) δ 201.4, 196.6, 172.7, 163.0, 163.0–161.1, 157.2, 156.8, 150.7, 149.2, 134.4–134.4, 126.8–126.7, 117.1–117.0, 110.6, 106.9, 104.8, 101.7, 90.3, 60.3, 31.5, 30.6, 13.5, 8.0. HRMS (ESI) *m/z* 433.1205 [M - H]$^-$ (calcd for 433.1209, $C_{24}H_{19}FN_2O_5$).

*4.2.4.4. (R)-8-acetyl-1-(4-(tert-butyl)phenyl)-5,7-dihydroxy-3,4a,6-trimethyl-1,4a-dihydro-4H-benzofuro[3,2-f]indazol-4-one. (**29**).* Yield 91%, yellow powder. m.p. 247–249 °C. ^{1}H NMR (500 MHz, DMSO-d_6) δ 13.37 (s, 1H), 11.26 (s, 1H), 7.60 (m, 4H), 6.58 (s, 1H), 2.65 (s, 3H), 2.48 (s, 3H), 2.00 (s, 3H), 1.77 (s, 3H), 1.35 (s, 9H). ^{13}C NMR (126 MHz, DMSO-d_6) δ 201.5, 196.7, 172.6, 163.0, 157.3, 156.9, 151.7, 150.7, 148.8, 135.6, 126.9, 123.9, 110.6, 106.9, 104.9, 101.7, 90.5, 60.2, 35.0, 31.5, 30.5, 13.6, 8.0. HRMS (ESI) *m/z* 471.1925 [M - H]$^-$ (calcd for 471.1922, $C_{28}H_{28}N_2O_5$).

*4.2.4.5. (R)-4-(8-acetyl-5,7-dihydroxy-3,4a,6-trimethyl-4-oxo-4,4a-dihydro-1H-benzofuro[3,2-f]indazol-1-yl)benzoic acid. (**30**).* Yield 63%, yellow powder. m.p. 181–182 °C. ^{1}H NMR (500 MHz, DMSO-d_6) δ 13.34 (s, 1H), 13.18 (bs, 1H), 11.14 (s, 1H), 8.14 (d, J = 8.6 Hz, 2H), 7.81 (d, J = 8.6 Hz, 2H), 6.68 (s, 1H), 2.63 (s, 3H), 2.50 (s, 3H), 1.98 (s, 3H), 1.77 (s, 3H). ^{13}C NMR (126 MHz, DMSO-d_6) δ 201.4, 196.7, 173.0, 166.9, 163.0, 157.2, 156.8, 151.2, 149.3, 141.3, 131.3, 130.8, 123.9, 111.0, 106.9, 104.8, 101.7, 90.6, 60.4, 31.5, 30.5, 13.5, 8.0. HRMS (ESI) *m/z* 459.1198 [M - H]$^-$ (calcd for 459.1211, $C_{25}H_{20}N_2O_7$).

*4.2.4.6. (R)-3-(8-acetyl-5,7-dihydroxy-3,4a,6-trimethyl-4-oxo-4,4a-dihydro-1H-benzofuro[3,2-f]indazol-1-yl)benzoic acid. (**31**).* Yield 71%, yellow powder. m.p. 167–169 °C. ^{1}H NMR (500 MHz, DMSO-d_6) δ 13.34 (s, 2H), 11.17 (s, 1H), 8.15 (d, J = 2.0 Hz, 1H), 8.05 (dt, J = 7.8, 1.3 Hz, 1H), 7.93 (ddd, J = 8.0, 2.3, 1.1 Hz, 1H), 7.74 (t, J = 7.9 Hz, 1H), 6.59 (s, 1H), 2.63 (s, 3H), 2.49 (s, 3H), 1.97 (s, 3H), 1.77 (s, 3H). ^{13}C NMR (126 MHz, DMSO-d_6) δ 201.4, 196.7, 172.9, 166.8, 163.0, 157.2, 156.8, 151.0, 149.2, 138.2, 132.8, 130.7, 129.6, 128.3, 124.7, 110.8, 106.9, 104.8, 101.7, 90.3, 60.3, 31.5, 30.5, 13.5, 7.9. HRMS (ESI) *m/z* 459.1198 [M - H]$^-$ (calcd for 459.1208, $C_{25}H_{20}N_2O_7$).

*4.2.4.7. (R)-2-(8-acetyl-5,7-dihydroxy-3,4a,6-trimethyl-4-oxo-4,4a-dihydro-1H-benzofuro[3,2-f]indazol-1-yl)benzoic acid. (**32**).* Yield 69%, yellow powder. m.p. 248–249 °C. ^{1}H NMR (500 MHz, DMSO-d_6) δ 13.36 (s, 1H), 13.21 (s, 1H), 11.28 (s, 1H), 8.00 (dd, J = 7.8, 1.4 Hz, 1H), 7.80 (td, J = 7.7, 1.5 Hz, 1H), 7.75–7.54 (m, 2H), 6.24 (s, 1H), 2.61 (s, 3H), 2.46 (s, 3H), 2.00 (s, 3H), 1.75 (s, 3H). ^{13}C NMR (126 MHz, DMSO-d_6) δ 201.5, 196.5, 172.5, 166.7, 163.0, 157.3, 156.9, 151.2, 149.9, 136.5, 133.4, 131.4, 130.5, 129.6, 128.7, 110.0, 106.9, 104.6, 101.7, 89.8, 60.3, 31.5, 30.9, 13.5, 8.0. HRMS (ESI) *m/z* 459.1198 [M - H]$^-$ (calcd for 459.1198, $C_{25}H_{20}N_2O_7$).

*4.2.4.8. Ethyl (R)-4-(8-acetyl-5,7-dihydroxy-3,4a,6-trimethyl-4-oxo-4,4a-dihydro-1H-benzofuro[3,2-f]indazol-1-yl)benzoate. (**33**).* Yield 66%, bright yellow powder. m.p. 226–227 °C. ^{1}H NMR (500 MHz, DMSO-d_6) δ 13.37 (s, 1H), 11.16 (s, 1H), 8.16 (d, J = 8.6 Hz, 2H), 7.85 (d, J = 8.6 Hz, 2H), 6.71 (s, 1H), 4.37 (q, J = 7.1 Hz, 2H), 2.65 (s, 3H), 2.50 (s, 3H), 2.00 (s, 3H), 1.78 (s, 3H), 1.36 (t, J = 7.1 Hz, 3H). ^{13}C NMR (126 MHz, DMSO-d_6) δ 201.4, 196.8, 173.2, 165.4, 163.0, 157.2, 156.8, 151.3, 149.4, 141.6, 131.2, 129.8, 124.1, 111.1, 107.0, 104.9, 101.7, 90.6, 61.6, 60.4, 31.5, 30.5, 14.7, 13.5, 8.0. HRMS (ESI) *m/z* 487.1511 [M - H]$^-$ (calcd for 487.1511, $C_{27}H_{24}N_2O_7$).

*4.2.4.9. (R)-8-acetyl-5,7-dihydroxy-1-(4-methoxyphenyl)-3,4a,6-trimethyl-1,4a-dihydro-4H-benzofuro[3,2-f]indazol-4-one. (**34**).* Yield 42%, yellow powder. m.p. 211–212 °C. ^{1}H NMR (600 MHz, DMSO-d_6) δ 13.38 (s, 1H), 11.29 (s, 1H), 7.58 (d, J = 8.9 Hz, 2H), 7.14 (d, J = 8.9 Hz, 2H), 6.49 (s, 1H), 3.85 (s, 3H), 2.64 (s, 3H), 2.47 (s, 3H), 1.99 (s, 3H), 1.76 (s, 3H). ^{13}C NMR (126 MHz, DMSO-d_6) δ 201.5, 196.6, 172.4, 162.9, 159.7, 157.3, 156.9, 150.4, 148.8, 131.0, 126.0, 115.2, 110.4, 106.8, 104.9, 101.7, 90.4, 60.2, 56.1, 31.5, 30.6, 13.5, 8.0. HRMS (ESI) *m/z* 445.1405 [M - H]$^-$ (calcd for 445.1400, $C_{25}H_{22}N_2O_6$).

*4.2.4.10. (R)-8-acetyl-5,7-dihydroxy-1-(3-methoxyphenyl)-3,4a,6-trimethyl-1,4a-dihydro-4H-benzofuro[3,2-f]indazol-4-one. (**35**).* Yield 47%, bright yellow powder. m.p. 95–97 °C. ^{1}H NMR (500 MHz, DMSO-d_6) δ 13.35 (s, 1H), 11.21 (s, 1H), 7.51 (t, J = 8.1 Hz, 1H), 7.30–6.98 (m, 3H), 6.57 (s, 1H), 3.85 (s, 3H), 2.63 (s, 3H), 2.48 (s, 3H), 1.98 (s, 3H), 1.76 (s, 3H). ^{13}C NMR (126 MHz, DMSO-d_6) δ 201.4, 196.7, 172.7, 163.0, 160.5, 157.2, 156.8, 150.7, 149.1, 139.1, 131.0, 116.5, 115.0, 110.7, 109.9, 106.9, 104.8, 101.7, 90.5, 60.3, 56.1, 31.5, 30.6, 13.5, 8.0.

HRMS (ESI) *m/z* 445.1405 [M - H]$^-$ (calcd for 445.1402, $C_{25}H_{22}N_2O_6$).

*4.2.4.11. (R)-8-acetyl-5,7-dihydroxy-3,4a,6-trimethyl-1-(4-(methylsulfonyl)phenyl)-1,4a-dihydro-4H-benzofuro[3,2-f]indazol-4-one. (**36**).* Yield 74%, yellow powder. m.p. 163–164 °C. ^{1}H NMR (600 MHz, DMSO-d_6) δ 13.34 (s, 1H), 11.11 (s, 1H), 8.23–8.08 (m, 2H), 8.05–7.85 (m, 2H), 6.72 (s, 1H), 3.32 (s, 3H), 2.62 (s, 3H), 2.51 (s, 4H), 1.97 (s, 3H), 1.77 (s, 3H). ^{13}C NMR (126 MHz, DMSO-d_6) δ 201.3, 196.8, 173.2, 163.0, 157.1, 156.7, 151.5, 149.7, 141.8, 140.6, 129.3, 124.7, 111.2, 107.0, 104.8, 101.7, 90.5, 60.4, 44.0, 31.5, 30.5, 13.5, 8.0. HRMS (ESI) *m/z* 493.1075 [M - H]$^-$ (calcd for 493.1082, $C_{25}H_{22}N_2O_7S$).

*4.2.4.12. (R)-4-(8-acetyl-5,7-dihydroxy-3,4a,6-trimethyl-4-oxo-4,4a-dihydro-1H-benzofuro[3,2-f]indazol-1-yl)benzenesulfonamide. (**37**).* Yield 79%, yellow powder. m.p. 298–299 °C. ^{1}H NMR (500 MHz, DMSO-d_6) δ 13.36 (s, 1H), 11.16 (s, 1H), 8.03 (d, J = 8.6 Hz, 2H), 7.90 (d, J = 8.7 Hz, 2H), 7.56 (s, 2H), 6.72 (s, 1H), 2.64 (s, 3H), 2.50 (s, 3H), 1.99 (s, 3H), 1.78 (s, 3H). ^{13}C NMR (126 MHz, DMSO-d_6) δ 201.4, 196.8, 173.2, 163.0, 157.2, 156.8, 151.3, 149.4, 144.1, 140.3, 127.8, 124.5, 111.1, 107.0, 104.9, 101.7, 90.6, 60.4, 31.5, 30.5, 13.5, 8.0. HRMS (ESI) *m/z* 494.1027 [M - H]$^-$ (calcd for 494.1031, $C_{24}H_{21}N_3O_7S$).

*4.2.4.13. (R)-8-acetyl-5,7-dihydroxy-3,4a,6-trimethyl-1-(pyridin-4-yl)-1,4a-dihydro-4H-benzofuro[3,2-f]indazol-4-one. (**38**).* Yield 83%, tawny powder. m.p. 248–250 °C. ^{1}H NMR (500 MHz, DMSO-d_6) δ 13.39 (s, 1H), 11.11 (s, 1H), 8.60 (dd, J = 5.0, 1.8 Hz, 1H), 8.08 (td, J = 7.9, 1.9 Hz, 1H), 7.96 (d, J = 8.3 Hz, 1H), 7.51–7.46 (m, 1H), 7.45 (s, 1H), 2.69 (s, 3H), 2.51 (s, 3H), 2.00 (s, 3H), 1.74 (s, 3H). ^{13}C NMR (126 MHz, DMSO-d_6) δ 201.5, 196.9, 172.9, 163.0, 157.1, 156.9, 152.2, 151.1, 149.2, 148.8, 140.3, 123.4, 115.6, 111.6, 107.0, 104.9, 101.8, 93.0, 60.4, 31.7, 30.6, 13.7, 8.0. HRMS (ESI) *m/z* 416.1252 [M - H]$^-$ (calcd for 416.1272, $C_{23}H_{19}N_3O_5$).

*4.2.4.14. (R)-8-acetyl-5,7-dihydroxy-3,4a,6-trimethyl-1-(pyridin-3-yl)-1,4a-dihydro-4H-benzofuro[3,2-f]indazol-4-one. (**39**).* Yield 75%, yellow powder. m.p. 121–122 °C. ^{1}H NMR (500 MHz, DMSO-d_6) δ 13.34 (s, 1H), 11.15 (s, 1H), 8.91 (d, J = 2.6 Hz, 1H), 8.82–8.60 (m, 1H), 8.14 (dt, J = 8.2, 2.0 Hz, 1H), 7.66 (dd, J = 8.2, 4.8 Hz, 1H), 6.68 (s, 1H), 2.63 (s, 3H), 2.50 (s, 3H), 1.98 (s, 3H), 1.76 (s, 3H). ^{13}C NMR (126 MHz, DMSO-d_6) δ 201.4, 196.7, 173.0, 163.0, 157.2, 156.8, 151.3, 149.9, 149.8, 145.1, 134.8, 132.1, 124.9, 110.9, 106.9, 104.8, 101.7, 90.3, 60.4, 31.5, 30.5, 13.5, 8.0. HRMS (ESI) *m/z* 416.1252 [M - H]$^-$ (calcd for 416.1273, $C_{23}H_{19}N_3O_5$).

*4.2.4.15. (R)-8-acetyl-5,7-dihydroxy-3,4a,6-trimethyl-1-(pyridin-2-yl)-1,4a-dihydro-4H-benzofuro[3,2-f]indazol-4-one. (**40**).* Yield 68%, bright yellow powder. m.p. 210–211 °C. ^{1}H NMR (500 MHz, DMSO-d_6) δ 13.39 (s, 1H), 11.11 (s, 1H), 8.65–8.52 (m, 1H), 8.08 (m, 1H), 8.02–7.91 (m, 1H), 7.48 (m, 1H), 7.46 (s, 1H), 2.69 (s, 3H), 2.50 (s, 3H), 2.00 (s, 3H), 1.74 (s, 3H). ^{13}C NMR (126 MHz, DMSO-d_6) δ 201.5, 196.9, 172.9, 163.0, 157.1, 156.9, 152.2, 151.1, 149.2, 148.8, 140.3, 123.4, 115.6, 111.6, 106.9, 104.9, 101.8, 93.0, 60.4, 31.7, 30.6, 13.7, 8.0. HRMS (ESI) *m/z* 416.1252 [M - H]$^-$ (calcd for 416.1254, $C_{23}H_{19}N_3O_5$).

*4.2.4.16. (R)-8-acetyl-5,7-dihydroxy-1-(6-methoxypyridin-3-yl)-3,4a,6-trimethyl-1,4a-dihydro-4H-benzofuro[3,2-f]indazol-4-one. (**41**).* Yield 40%, yellow powder. m.p. 196–197 °C. ^{1}H NMR (500 MHz, DMSO-d_6) δ 13.35 (s, 1H), 11.21 (s, 1H), 8.47 (d, J = 2.8 Hz, 1H), 8.01 (dd, J = 8.8, 2.8 Hz, 1H), 7.04 (d, J = 8.8 Hz, 1H), 6.58 (s, 1H), 3.95 (s, 3H), 2.63 (s, 3H), 2.48 (s, 3H), 1.98 (s, 3H), 1.75 (s, 3H). ^{13}C NMR (126 MHz, DMSO-d_6) δ 201.4, 196.6, 172.7, 163.7, 163.0, 157.2, 156.8, 150.9, 149.7, 143.0, 136.1, 129.3, 111.8, 110.5, 106.9, 104.8, 101.7, 90.2, 60.3, 54.3, 31.5, 30.6, 13.5, 8.0. HRMS (ESI) *m/z* 446.1358 [M - H]$^-$ (calcd for 446.1357, $C_{24}H_{21}N_3O_6$).

*4.2.4.17. (R)-8-acetyl-5,7-dihydroxy-3,4a,6-trimethyl-1-(6-methylpyridazin-3-yl)-1,4a-dihydro-4H-benzofuro[3,2-f]indazol-4-one. (**42**).* Yield 58%, bright yellow powder. m.p. 242–243 °C. ^{1}H NMR (600 MHz, DMSO-d_6) δ 13.37 (s, 1H), 11.01 (s, 1H), 8.12 (d, J = 9.0 Hz, 1H), 7.86 (d, J = 9.0 Hz, 1H), 7.37 (s, 1H), 2.70 (s, 3H), 2.68 (s, 3H), 2.51 (s, 3H), 2.00 (s, 3H), 1.74 (s, 3H). ^{13}C NMR (126 MHz, DMSO-d_6) δ 201.5, 197.0, 173.4, 163.0, 160.2, 157.1, 156.8, 154.8, 151.6, 149.6, 131.1, 120.8, 111.9, 107.0, 104.8, 101.8, 92.6, 60.6, 31.6, 30.6, 21.8, 13.7, 8.0. HRMS (ESI) *m/z* 431.1361 [M - H]$^-$ (calcd for 431.1360, $C_{23}H_{20}N_4O_5$).

*4.2.4.18. (R)-8-acetyl-5,7-dihydroxy-3,4a,6-trimethyl-1-(pyrazin-2-yl)-1,4a-dihydro-4H-benzofuro[3,2-f]indazol-4-one. (**43**).* Yield 73%, pale yellow powder. m.p. 230–232 °C. ^{1}H NMR (500 MHz, DMSO-d_6) δ 13.36 (s, 1H), 10.99 (s, 1H), 9.21 (d, J = 1.3 Hz, 1H), 8.73 (d, J = 2.6 Hz, 1H), 8.67 (dd, J = 2.5, 1.4 Hz, 1H), 7.34 (s, 1H), 2.68 (s, 3H), 2.52 (s, 3H), 1.99 (s, 3H), 1.74 (s, 3H). ^{13}C NMR (126 MHz, DMSO-d_6) δ 201.4, 196.8, 173.4, 163.0, 157.0, 156.8, 151.8, 150.3, 148.3, 143.6, 142.8, 137.6, 111.8, 107.1, 104.8, 101.8, 92.3, 60.7, 31.6, 30.6, 13.6, 8.0. HRMS (ESI) *m/z* 417.1204 [M - H]$^-$ (calcd for 417.1223, $C_{22}H_{18}N_4O_5$).

*4.2.4.19. (R)-4-(8-acetyl-5,7-dihydroxy-3,4a,6-trimethyl-4-oxo-4,4a-dihydro-1H-benzofuro[3,2-f]indazol-1-yl)benzonitrile. (**44**).* Yield 37%, yellow powder. m.p. 136–137 °C. ^{1}H NMR (500 MHz, DMSO-d_6) δ 13.34 (s, 1H), 11.10 (s, 1H), 8.08 (d, J = 8.5 Hz, 2H), 7.90 (d, J = 8.5 Hz, 2H), 6.70 (s, 1H), 2.64 (s, 3H), 2.49 (s, 3H), 1.98 (s, 3H), 1.77 (s, 3H). ^{13}C NMR (126 MHz, DMSO-d_6) δ 201.4, 196.8, 173.3, 163.0, 157.1, 156.8, 151.5, 149.7, 141.5, 134.5, 124.8, 118.6, 111.2, 111.2, 107.0, 104.8, 101.7, 90.6, 60.5, 31.5, 30.5, 13.5, 8.0. HRMS (ESI) *m/z* 440.1252 [M - H]$^-$ (calcd for 440.1256, $C_{25}H_{19}N_3O_5$).

*4.2.4.20. (R)-8-acetyl-1-(1H-benzo[d]imidazol-2-yl)-5,7-dihydroxy-3,4a,6-trimethyl-1,4a-dihydro-4H-benzofuro[3,2-f]indazol-4-one. (**45**).* Yield 62%, yellow powder. m.p. 246–248 °C. ^{1}H NMR (500 MHz, DMSO-d_6) δ 13.37 (s, 1H), 13.28 (bs, 1H), 11.01 (s, 1H), 7.66 (m, 1H), 7.49 (m, 2H), 7.24 (m, 2H), 2.71 (s, 3H), 2.55 (s, 3H), 2.00 (s, 3H), 1.75 (s, 3H). ^{13}C NMR (126 MHz, DMSO-d_6) δ 201.5, 196.6, 174.0, 163.0, 157.0, 156.8, 151.8, 149.9, 145.5, 142.1, 133.3, 123.4, 122.8, 119.1, 112.2, 111.5, 107.1, 104.9, 101.8, 91.7, 61.0, 31.7, 30.8, 13.6, 8.0. HRMS (ESI) *m/z* 455.1361 [M - H]$^-$ (calcd for 455.1361, $C_{25}H_{20}N_4O_5$).

*4.2.4.21. (R)-8-acetyl-1-(benzo[d]thiazol-2-yl)-5,7-dihydroxy-3,4a,6-trimethyl-1,4a-dihydro-4H-benzofuro[3,2-f]indazol-4-one. (**46**).* Yield 88%, yellow powder. m.p. 281–282 °C. ^{1}H NMR (600 MHz, Chloroform-*d*) δ 13.34 (s, 1H), 10.80 (s, 1H), 7.96 (d, J = 8.2 Hz, 1H), 7.85 (d, J = 7.9 Hz, 1H), 7.54–7.45 (m, 2H), 7.39 (td, J = 7.6, 1.1 Hz, 1H), 2.74 (s, 3H), 2.58 (s, 3H), 2.11 (s, 3H), 1.79 (s, 3H). ^{13}C NMR (151 MHz, Chloroform-*d*) δ 200.5, 196.2, 174.8, 163.7, 159.8, 157.3, 156.3, 1529, 151.0, 149.6, 132.7, 126.8, 125.5, 122.8, 121.5, 112.0, 108.6, 103.8, 101.7, 91.4, 61.3, 31.4, 30.8, 13.3, 7.5.

*4.2.4.22. (R)-8-acetyl-5,7-dihydroxy-3,4a,6-trimethyl-1-(4-oxo-3,4-dihydrophthalazin-1-yl)-1,4a-dihydro-4H-benzofuro[3,2-f]indazol-4-one. (**47**).* Yield 33%, tawny powder. m.p. 315–316 °C. ^{1}H NMR (600 MHz, DMSO-d_6) δ 13.36 (s, 1H), 13.05 (s, 1H), 11.16 (s, 1H), 8.40–8.29 (m, 1H), 8.12–7.92 (m, 2H), 7.88–7.64 (m, 1H), 6.75 (s, 1H), 2.60 (s, 3H), 2.54 (s, 3H), 2.00 (s, 3H), 1.76 (s, 3H). ^{13}C NMR (151 MHz, DMSO-d_6) δ 201.4, 196.9, 172.9, 162.9, 160.0, 157.1, 156.8, 152.2, 151.1, 138.2, 134.6, 133.3, 129.1, 127.2, 126.8, 125.4, 110.2, 106.9, 104.9, 101.7, 90.4, 60.5, 31.4, 30.6, 13.6, 8.0. HRMS (ESI) *m/z* 483.1310 [M - H]$^-$ (calcd for 483.1319, $C_{26}H_{20}N_4O_6$).

*4.2.4.23. (R)-8-acetyl-5,7-dihydroxy-3,4a,6-trimethyl-1-(phenylsulfonyl)-1,4a-dihydro-4H-benzofuro[3,2-f]indazol-4-one. (**48**).*

Yield 93%, yellow powder. m.p. 208–209 °C. ^{1}H NMR (600 MHz, DMSO-d_6) δ 13.36 (s, 1H), 10.68 (s, 1H), 8.19–8.05 (m, 2H), 7.90–7.81 (m, 1H), 7.73 (t, J = 7.8 Hz, 2H), 7.06 (s, 1H), 2.72 (s, 3H), 2.37 (s, 3H), 1.98 (s, 3H), 1.69 (s, 3H). ^{13}C NMR (151 MHz, DMSO-d_6) δ 201.5, 196.9, 175.6, 162.9, 156.7, 156.6, 153.2, 152.9, 136.4, 136.2, 130.7, 128.5, 111.6, 107.2, 105.0, 101.8, 90.1, 61.2, 31.6, 30.5, 13.6, 8.0. HRMS (ESI) m/z 479.0918 [M - H]$^-$ (calcd for 479.0927, $C_{24}H_{20}N_2O_7S$).

*4.2.4.24. (R)-8-acetyl-5,7-dihydroxy-3,4a,6-trimethyl-1-tosyl-1,4a-dihydro-4H-benzofuro[3,2-f]indazol-4-one. (**49**).* Yield 95%, yellow powder. m.p. 221–222 °C. ^{1}H NMR (500 MHz, DMSO-d_6) δ 13.36 (s, 1H), 10.71 (s, 1H), 7.99 (d, J = 8.2 Hz, 2H), 7.52 (d, J = 8.2 Hz, 2H), 7.05 (s, 1H), 2.72 (s, 3H), 2.41 (s, 3H), 2.36 (s, 3H), 1.99 (s, 3H), 1.69 (s, 3H). ^{13}C NMR (126 MHz, DMSO-d_6) δ 201.5, 197.0, 175.5, 162.9, 156.8, 156.6, 153.0, 152.7, 147.5, 133.3, 131.2, 128.6, 111.5, 107.2, 105.1, 101.9, 90.2, 61.2, 31.7, 30.5, 21.7, 13.6, 8.0. HRMS (ESI) m/z 493.1075 [M - H]$^-$ (calcd for 493.1071, $C_{25}H_{22}N_2O_7S$).

*4.2.4.25. (R)-8-acetyl-5,7-dihydroxy-1-((4-methoxyphenyl)sulfonyl)-3,4a,6-trimethyl-1,4a-dihydro-4H-benzofuro[3,2-f]indazol-4-one. (**50**).* Yield 94%, yellow powder. m.p. 200–201 °C. ^{1}H NMR (500 MHz, DMSO-d_6) δ 13.37 (s, 1H), 10.73 (s, 1H), 8.06 (d, J = 9.0 Hz, 2H), 7.22 (d, J = 9.0 Hz, 2H), 7.06 (s, 1H), 3.87 (s, 3H), 2.72 (s, 3H), 2.37 (s, 3H), 1.99 (s, 3H), 1.69 (s, 3H). ^{13}C NMR (126 MHz, DMSO-d_6) δ 201.5, 197.0, 175.3, 165.3, 162.9, 156.8, 156.6, 152.8, 152.4, 131.2, 127.2, 115.9, 111.4, 107.2, 105.1, 101.8, 90.2, 61.1, 56.6, 31.7, 30.6, 13.6, 8.0. HRMS (ESI) m/z 509.1024 [M - H]$^-$ (calcd for 509.1041, $C_{25}H_{22}N_2O_8S$).

4.3. Biology

4.3.1. AcPHF6 aggregation kinetics by Thioflavin T fluorescence assays

ThT fluorescence assays were performed as described previously [58,62,63] with some variations. The AcPHF6 powder (MedChemExpress) was first dissolved in 1,1,1,3,3,3,-hexafluoro-2-propanol (HFIP), dispensed and ventilated overnight at room temperature. The AcPHF6 (1 mM) stock solution was formulated with pure water and immediately used in ThT fluorescence experiments. All test compounds were prepared in DMSO with 10 mM stock solution, while stock solution of 10 mM ThT (MedChemExpress) was prepared in 50 mM phosphate buffer pH 7.4. AcPHF6 aggregation was detected by fluorescence microplate reader in a black 96-well optical flat-bottom plate, and the excitation and emission wavelengths were set to 440 nm and 490 nm, respectively. The total volume of each well was 100 μL for a final concentration of 100 μM AcPHF6, 20 μM ThT and 10 μM usnic acid derivatives (maximum final DMSO content: 0.1%, v/v) in 50 mM phosphate buffer pH 7.4. In addition, 10 μM myricetin (MedChemExpress) was used as a positive control and compound-free wells were added DMSO as a negative control and sodium usnate (Yuanye, Shanghai, China) was also used as a reference. System temperature was set at 25 °C. Fluorescence data were recorded every minute over 120 min with 10 s shaking (400 rpm) prior to each reading. At least three parallel wells are set for each compound, and the fluorescence values between 50 and 60 min are finally averaged to calculate the inhibition rate (%). Results are expressed as the mean ± SD of three independent experiments.

4.3.2. Circular dichroism (CD) spectroscopy

CD spectra were measured in the 260-200 nm spectral range on a Jasco J-810 spectropolarimeter (Jasco Corporation, Tokyo, Japan) using a quartz small cell with a path length of 1 mm and a maximum volume of 300 μL. Measurement informations were recorded at room temperature with a 1 s response, a 1 nm bandwidth, 1 nm data pitch and a 50 nm min^{-1} scanning speed. Spectra were acquired from fresh samples, which included a final concentration of 100 μM AcPHF6 and 10 μM compound **18** and **30** (maximum final DMSO content: 0.1%, v/v) in 50 mM phosphate buffer pH 7.4. CD spectra of the samples were measured immediately after vibration for 10 s per minute at 25 °C for 120 min. The spectral contribution of solvents and test compounds were deducted before converting the spectral raw data to molar units per residue ($\Delta\varepsilon_{res}$), and then spectral curves smoothed by Savitzky-Golay method.

4.3.3. Transmission electron microscopy (TEM)

The sample preparation method for TEM Assay was same as that for the CD assay. In order to facilitate the observation of the filaments, the final concentration of AcPHF6 was increased to 200 μM, but the concentration ratio of protein to compound **30** (20 μM) remained unchanged. Samples (10 μL) were placed on a carbon-coated copper grid for 5 min. Each grid was stained with phosphotungstic acid (1%, 10 μL) for 5 min. After draining excess dye solution and drying it, the specimen was transferred for imaging in a Hitachi HT7700 transmission electron microscope (Hitachi, Tokyo, Japan).

4.3.4. Full-length 2N4R tau protein expression and purification

Full-length 2N4R tau protein was purified by previously published method [66]. Briefly, the full-length 2N4R tau was cloned into pET-28a vector (Novagen) to produce a His-tagged protein in *Escherichia coli* strain BL21 (DE3). When vector-transformed bacteria grown to an optical density (OD) of 0.6 at 600 nm, isopropyl-beta-Dthiogalactopyranoside (IPTG) was used at a final concentration of 1 mM to induce 2N4R tau expression at 37 °C. After 4 h, the bacteria were collected and lysed. Bacterial lysates were loaded on the His-hag purification resin (Sigma-Aldrich, U.S.), and the heteroprotein was washed out with low-density imidazole (20 mM) in PBS 1 × , then the target tau protein was washed out with high-density imidazole (200 mM) in PBS 1 × . Purity of the protein was verified on a Coomassie Brilliant Blue stained SDS-polyacrylamide gel. 2N4R tau protein was concentrated by an ultrafiltration tube (Millipore, U.S.), and then the protein concentration was determined by the BCA method. Full-length 2N4R tau protein was stored at −80 °C until use.

4.3.5. Full-length 2N4R tau protein aggregation kinetics

Full-length 2N4R tau protein solution (10 μM) was incubated at 37 °C in the presence of 10 μM compound **30** and 1 mM DTT, 10 μM heparin (Average molecular weight: 6117) was added to initiate the reaction in PBS 1 × , and 10 μM ThT dye (all from MedChemExpress) was added to detect the aggregation progress. A basic reaction mixture was performed in a black 96-well optical flat-bottom plate. The plate was inserted into a fluorescent plate reader, and the excitation and the emission wavelengths were set to 440 nm and 490 nm, respectively. The reading period was 4 min and shaked (600 rpm) for 2 min before reading.

4.3.6. Cytotoxicity test

The toxicity effect of compound **30** on the Human neuroblastoma SK-N-SH cell line (SH-SY5Y), human hepatocyte cells (LO2) cells and BV2 microglial cells was examined. The cells were routinely grown in high glucose DMEM supplemented with 10% fetal bovine serum, 100 units/mL penicillin, and 100 units/mL of streptomycin in a humidified incubator with 5% CO_2 at 37 °C. Cells were subcultured in 96-well plates at a seeding density of 3000–5000 cells per well and allowed to adhere and grow. When the cells reached the desired confluence, they were incubated with the compounds at the required concentration and incubated for

another 24 h. Subsequently, cells were incubated with 20 μL of 0.5 mg/mL MTT solution for 4 h at 37 °C and 5% CO_2. Then removed all media and added 200 μL of DMSO to dissolve the formazan crystals attached to the bottom of the plate. The absorbance of each well was measured using a microculture plate reader with a test wavelength of 570 nm and a reference wavelength of 630 nm. Results are expressed as the mean ± SD of three independent experiments.

4.3.7. Inhibiting NO production of LPS-stimulated BV2 microglial cells

BV2 microglia cells were routinely grown in high glucose DMEM supplemented with 10% fetal bovine serum, 100 units/mL penicillin, and 100 units/mL of streptomycin in a humidified incubator with 5% CO_2 at 37 °C. When the cells reached the desired confluence, they were seeded in a 96-well microplate at a density of 3×10^4 cells/well. After the cells attached, cells were preincubated with the compounds at the desired concentration for 1 h and after that time LPS (Sigma-Aldrich, U.S.) was added at a final concentration of 1 μg/ml and incubated for another 18 h. 50 μL of medium was transferred to a new 96-well plate, then added the same volume of Griess assay reagent and incubated for 10 min at 25 °C. Immediately, the absorbance at 540 nm was measured in a multifunction microplate reader. Calculate the percent inhibition of NO production by the formula: $(F_L\text{-}F_C)/(F_L\text{-}F_0) \times 100$, where F_C is absorbance of the neurons treated with the tested compound, F_L is absorbance of the neurons treated with LPS, and F_0 is absorbance of the normal neurons.Results are expressed as the mean ± SD of three independent experiments.

4.3.8. Animal study

Adult male SD rats (250–270 g), were purchased from Shanghai Sippr Bk Laboratory Animals Ltd (Shanghai, China). The rats were reared on a 12/12 h light/dark cycle at 25 °C, 60–70% relative humidity and allowed free access to water and standard chow ad lib. Animals were reared and handled strictly according to the obligations of the Animal Ethics Committee of China Pharmaceutical University and the guidelines for the care and use of laboratory animal from the National Institute of Health. Sterile food and water were provided according to institutional guidelines. The animals were acclimated for 7 days prior to operation.

4.3.8.1. Animal modeling. Animal modeling was performed by previously published method [67]. Rats were anesthetized with isoflurane and placed in a stereotaxic apparatus. Okadiac acid (300 ng in 1.5 μL of saline) or saline (0.9% NaCl,1.5 μL) was microinjected stereotaxically by micro syringe (8 mm diameter) into the right dorsal hippocampus (−3.8 mm AP, −2.5 mm ML, and −3.2 mm DV, according to the Rat Brain Paxinos Atlas) and completed in 5–6 min. Then, the needle remained stationary for 5 min to ensure OA diffusion and removed slowly over 5 min. Finally, the wound of the rats was sutured and wiped with penicillin (50 mg/mL) for 3 days to prevent wound infection. Rats injected with OA and saline were regarded as model group and control group, respectively. Subsequent subdivision of the model group based on the treatment of the drugs.

4.3.8.2. Drug injection and animal grouping. After 7 days of adaptive feeding, rats with a body weight of 260–280 g were randomly selected and divided into 4 groups (n = 8 per group): control (sham operation), model, **30** (5 mg/kg), **30** (10 mg/kg). Due to the poor water solubility of **30**, 8% DMSO and 1% Tween-80 were used as a cosolvent and dissolved in physiological saline. **30** 5 mg/kg group and **30** 10 mg/kg group were intraperitoneally injected with the corresponding doses according to body weight for 7 days, during which the control group and the model group were only injected with physiological saline and cosolvent. Subsequently, rats were modeled and the control group was only sham operated. The Morris water maze test was performed 7 days after the treatment. Rats body weight changes were recorded during the period.

4.3.8.3. Morris water maze test. Spatial memory function of rats was tested by Morris water maze, it included 5 days of learning and memory training and a probe trial on day 6. Rats were individually trained in a circular pool (110 cm in diameter and 60 cm in height) filled with water to a depth of 40 cm and maintained at 25 °C with an automatic heater. The maze was located in a darker room but contained a mass of fixed visual cues. The circular pool was divided into four quadrants, where an escape platform was placed and fixed 1 cm below the surface of the water in the center of one of the quadrants. On the first 5 days, rats (n = 8 per group) were trained four times a day, each training randomly changed a quadrant where the rats were placed in the maze. If a rat successfully reached the platform (a successful escape) within 60 s, it was allowed to stay there for another 15 s. If not, it was directed to the platform and also stayed there for 15 s to ensure consistent learning time. In order to prevent a cold, every time the rats were removed from the water, they were dried with a towel. The swimming speed and the latencies to find the platform were recorded. On the last day (day 6), the platform was removed from its location, then rats were given a probe trial and they had 60 s to search for the platform. During the period, the rats were placed in the quadrant farthest from the virtual platform to start the examination. The time taken to reach the missing platform and the number of times the animals crossed the platform location were recorded. Data for the escape latency, the distances traveled, and the number of platform location crossings were recorded and processed by ananalysis-management system.

Declaration of competing interest

We declare that we do not have any commercial or associative interest that represents a conflict of interest in connection with the work submitted.

Acknowledgments

This work was supported by the National Natural Science Foundation of China (81573313), the “Double First-Class” University Project (CPU2018GF03), Jiangsu Province ‘333’ Project (Wang, X.B.), the Qinglan Project of Jiangsu Province of China (Wang, X. B.), the Six Talent Peaks Project of Jiangsu Province (SWYY-107), and the Innovative Research Team in University (IRT_15R63).

Appendix A. Supplementary data

Supplementary data to this article can be found online at https://doi.org/10.1016/j.ejmech.2019.111961.

References

[1] Alzheimer's disease facts and figures, Alzheimer's Dementia 14 (2018) 367–429, 2018.
[2] P. Scheltens, K. Blennow, M.M.B. Breteler, B. de Strooper, G.B. Frisoni, S. Salloway, W.M. Van der Flier, Alzheimer's disease, The Lancet 388 (2016) 505–517.
[3] I. Benilova, E. Karran, B. De Strooper, The toxic Abeta oligomer and Alzheimer's disease: an emperor in need of clothes, Nat. Neurosci. 15 (2012) 349–357.
[4] C. Ballatore, V.M. Lee, J.Q. Trojanowski, Tau-mediated neurodegeneration in Alzheimer's disease and related disorders, Nat. Rev. Neurosci. 8 (2007) 663–672.
[5] J. Emerit, M. Edeas, F. Bricaire, Neurodegenerative diseases and oxidative stress, Biomed. Pharmacother. 58 (2004) 39–46.

[6] A. Singh, A. Chokriwal, M.M. Sharma, D. Jain, J. Saxena, B.J. Stephen, Therapeutic role and drug delivery potential of neuroinflammation as a target in neurodegenerative disorders, ACS Chem. Neurosci. 8 (2017) 1645–1655.

[7] D. Drago, S. Bolognin, P. Zatta, Role of metal ions in the Aβ oligomerization in Alzheimer's disease and in other neurological disorders, Curr. Alzheimer Res. 5 (2008) 500–507.

[8] D.E. Kuhl, R.A. Koeppe, S. Minoshima, S.E. Snyder, E.P. Ficaro, N.L. Foster, K.A. Frey, M.R. Kilbourn, *In vivo* mapping of cerebral acetylcholinesterase activity in aging and Alzheimer's disease, Neurology 52 (1999) 691–699.

[9] F. Mangialasche, A. Solomon, B. Winblad, P. Mecocc, M. Kivipelto, Alzheimer's disease: clinical trials and drug development, Lancet Neurol. 9 (2010) 702–716.

[10] M.G. Savelieff, G. Nam, J. Kang, H.J. Lee, M. Lee, M.H. Lim, Development of multifunctional molecules as potential therapeutic candidates for alzheimer's disease, Parkinson's disease, and amyotrophic lateral sclerosis in the last decade, Chem. Rev. 119 (2019) 1221–1322.

[11] J. Cummings, G. Lee, A. Ritter, K. Zhong, Alzheimer's disease drug development pipeline, Alzheimers Dement (N Y) 4 (2018) 195–214, 2018.

[12] K. Herrup, The case for rejecting the amyloid cascade hypothesis, Nat. Neurosci. 18 (2015) 794–799.

[13] A.J. Doig, M.P. Del Castillo-Frias, O. Berthoumieu, B. Tarus, J. Nasica-Labouze, F. Sterpone, P.H. Nguyen, N.M. Hooper, P. Faller, P. Derreumaux, Why is Research on amyloid-beta failing to give new drugs for alzheimer's disease? ACS Chem. Neurosci. 8 (2017) 1435–1437.

[14] E. Giacobini, G. Gold, Alzheimer disease therapy-moving from amyloid-β to tau, Nat. Rev. Neurol. 9 (2013) 677–686.

[15] E.D. Roberson, K. Scearce-Levie, J.J. Palop, F. Yan, I.H. Cheng, T. Wu, H. Gerstein, G.Q. Yu, L. Mucke, Reducing endogenous tau ameliorates amyloid β-induced deficits in an alzheimer's disease mouse model, Science 316 (2007) 750–754.

[16] I. Koychev, R.N. Gunn, A. Firouzian, J. Lawson, G. Zamboni, B. Ridha, B.J. Sahakian, J.B. Rowe, A. Thomas, L. Rochester, D. Ffytche, R. Howard, H. Zetterberg, C. MacKay, S. Lovestone, Deep, t. Frequent phenotyping study, PET tau and amyloid-beta burden in mild alzheimer's disease: divergent relationship with age, cognition, and cerebrospinal fluid biomarkers, J. Alzheimer's Dis. 60 (2017) 283–293.

[17] M.R. Brier, B. Gordon, K. Friedrichsen, J. McCarthy, A. Stern, J. Christensen, C. Owen, P. Aldea, Y. Su, J. Hassenstab, N.J. Cairns, D.M. Holtzman, A.M. Fagan, J.C. Morris, T.L.S. Benzinger, B.M. Ances, Tau and Aβ imaging, CSF measures, and cognition in Alzheimer's disease, Sci. Transl. Med. 8 (2016), 338ra366.

[18] M.D. Weingarten, A.H. Lockwood, S.Y. Hwo, M.W. Kirschner, A protein factor essential for microtubule assembly, Proc. Natl. Acad. Sci. 72 (1975) 1858–1862.

[19] M. Goedert, D.S. Eisenberg, R.A. Crowther, Propagation of tau aggregates and neurodegeneration, Annu. Rev. Neurosci. 40 (2017) 189–210.

[20] F. Hernandez, J. Avila, Tauopathies, Cell. Mol. Life Sci. 64 (2007) 2219–2233.

[21] Y. Wang, E. Mandelkow, Tau in physiology and pathology, Nat. Rev. Neurosci. 17 (2016) 5–21.

[22] I. Grundke-Iqbal, K. Iqbal, Y.C. Tung, M. Quinlan, H.M. Wisniewski, L.I. Binder, Abnormal phosphorylation of the microtubule-associated protein tau (tau) in Alzheimer cytoskeletal pathology, Proc. Natl. Acad. Sci. 83 (1986) 4913–4917.

[23] G. Lindwall, R. David Cole, Phosphorylation affects the ability of tau protein to promote microtubule assembly, J. Biol. Chem. 259 (1984) 5301–5305.

[24] D. Chu, F. Liu, Pathological changes of tau related to alzheimer's disease, ACS Chem. Neurosci. 10 (2019) 931–944.

[25] K. Demaegd, J. Schymkowitz, F. Rousseau, Transcellular spreading of tau in tauopathies, Chembiochem 19 (2018) 2424–2432.

[26] B.B. Holmes, J.L. Furman, T.E. Mahan, T.R. Yamasaki, H. Mirbaha, W.C. Eades, L. Belaygorod, N.J. Cairns, D.M. Holtzman, M.I. Diamond, Proteopathic tau seeding predicts tauopathy *in vivo*, Proc. Natl. Acad. Sci. 111 (2014) E4367–E4385.

[27] P.V. Arriagada, J.H. Growdon, E.T. Hedleywhyte, B.T. Hyman, Neurofibrillary tangles but not senile plaques parallel duration and severity of Alzheimer's disease, Neurology 42 (1992) 631–639.

[28] H. Braak, E. Braak, Neuropathological stageing of Alzheimer-related changes, Acta Neuropathol. 82 (1991) 239–259.

[29] A.P. Saraswati, S.M. Ali Hussaini, N.H. Krishna, B.N. Babu, A. Kamal, Glycogen synthase kinase-3 and its inhibitors: potential target for various therapeutic conditions, Eur. J. Med. Chem. 144 (2018) 843–858.

[30] B. Bulic, M. Pickhardt, E. Mandelkow, Progress and developments in tau aggregation inhibitors for Alzheimer disease, J. Med. Chem. 56 (2013) 4135–4155.

[31] M.J. Metcalfe, M.E. Figueiredo-Pereira, Relationship between tau pathology and neuroinflammation in Alzheimer's disease, MSJM (Mt. Sinai J. Med.) 77 (2010) 50–58.

[32] C. Laurent, L. Buee, D. Blum, Tau and neuroinflammation: what impact for alzheimer's disease and tauopathies? Biomed. J. 41 (2018) 21–33.

[33] K.A. Walker, B.N. Ficek, R. Westbrook, Understanding the role of systemic inflammation in alzheimer's disease, ACS Chem. Neurosci. 10 (2019) 3340–3342.

[34] M.T. Heneka, M.J. Carson, J.E. Khoury, G.E. Landreth, F. Brosseron, D.L. Feinstein, A.H. Jacobs, T. Wyss-Coray, J. Vitorica, R.M. Ransohoff, K. Herrup, S.A. Frautschy, B. Finsen, G.C. Brown, A. Verkhratsky, K. Yamanaka, J. Koistinaho, E. Latz, A. Halle, G.C. Petzold, T. Town, D. Morgan, M.L. Shinohara, V.H. Perry, C. Holmes, N.G. Bazan, D.J. Brooks, S. Hunot, B. Joseph, N. Deigendesch, O. Garaschuk, E. Boddeke, C.A. Dinarello, J.C. Breitner, G.M. Cole, D.T. Golenbock, M.P. Kummer, Neuroinflammation in Alzheimer's disease, Lancet Neurol. 14 (2015) 388–405.

[35] J.M. Rubio-Perez, J.M. Morillas-Ruiz, A review: inflammatory process in Alzheimer's disease, role of cytokines, Sci. World J. (2012) 756357, 2012.

[36] I.C. Stancu, N. Cremers, H. Vanrusselt, J. Couturier, A. Vanoosthuyse, S. Kessels, C. Lodder, B. Brone, F. Huaux, J.N. Octave, D. Terwel, I. Dewachter, Aggregated Tau activates NLRP3-ASC inflammasome exacerbating exogenously seeded and non-exogenously seeded Tau pathology *in vivo*, Acta Neuropathol. 137 (2019) 599–617.

[37] B. Mravec, K. Lejavova, P. Vargovic, K. Ondicova, L. Horvathova, P. Novak, G. Manz, P. Filipcik, M. Novak, R. Kvetnansky, Tauopathy in transgenic (SHR72) rats impairs function of central noradrenergic system and promotes neuroinflammation, J. Neuroinflammation 13 (2016) 15.

[38] J.D. Cherry, Y. Tripodis, V.E. Alvarez, B. Huber, P.T. Kiernan, D.H. Daneshvar, J. Mez, P.H. Montenigro, T.M. Solomon, M.L. Alosco, R.A. Stern, A.C. McKee, T.D. Stein, Microglial neuroinflammation contributes to tau accumulation in chronic traumatic encephalopathy, Acta Neuropathol. Commun. 4 (2016) 112.

[39] M. Cocchietto, N. Skert, P.L. Nimis, G. Sava, A review on usnic acid, an interesting natural compound, Naturwissenschaften 89 (2002) 137–146.

[40] A.A. Araujo, M.G. de Melo, T.K. Rabelo, P.S. Nunes, S.L. Santos, M.R. Serafini, M.R. Santos, L.J. Quintans-Junior, D.P. Gelain, Review of the biological properties and toxicity of usnic acid, Nat. Prod. Res. 29 (2015) 2167–2180.

[41] O.A. Luzina, N.F. Salakhutdinov, Usnic acid and its derivatives for pharmaceutical use: a patent review (2000-2017), Expert Opin. Ther. Pat. 28 (2018) 477–491.

[42] Y. Yang, W.K. Bae, J.Y. Lee, Y.J. Choi, K.H. Lee, M.S. Park, Y.H. Yu, S.Y. Park, R. Zhou, I. Tas, C. Gamage, M.J. Paik, J.H. Lee, I.J. Chung, K.K. Kim, J.S. Hur, S.K. Kim, H.H. Ha, H. Kim, Potassium usnate, a water-soluble usnic acid salt, shows enhanced bioavailability and inhibits invasion and metastasis in colorectal cancer, Sci. Rep. 8 (2018) 16234.

[43] A.A. Shtro, V.V. Zarubaev, O.A. Luzina, D.N. Sokolov, O.I. Kiselev, N.F. Salakhutdinov, Novel derivatives of usnic acid effectively inhibiting reproduction of influenza A virus, Bioorg. Med. Chem. 22 (2014) 6826–6836.

[44] O.A. Luzina, M.P. Polovinka, N.F. Salakhutdinov, G.A. Tolstikov, Chemical modification of usnic acid: III.* Reaction of (+)-usnic acid with substituted phenylhydrazines, Russ. J. Org. Chem. 45 (2010) 1783–1789.

[45] P.F.M. Von Bergen, J. Biernat, E.-M. Mandelkow, E. Mandelkow, Assembly of tau protein into Alzheimer paired helical filaments depends on a local sequence motif (306VQIVYK311) forming beta structure, Proc. Natl. Acad. Sci. 97 (2000) 5129–5134.

[46] P. Ganguly, T.D. Do, L. Larini, N.E. LaPointe, A.J. Sercel, M.F. Shade, S.C. Feinstein, M.T. Bowers, J.E. Shea, Tau assembly: the dominant role of PHF6 (VQIVYK) in microtubule binding region repeat R3, J. Phys. Chem. B 119 (2015) 4582–4593.

[47] L. Lunven, H. Bonnet, S. Yahiaoui, W. Yi, L. Da Costa, M. Peuchmaur, A. Boumendjel, S. Chierici, Disruption of fibers from the tau model AcPHF6 by naturally occurring aurones and synthetic analogues, ACS Chem. Neurosci. 7 (2016) 995–1003.

[48] T. Mohamed, T. Hoang, M. Jelokhani-Niaraki, P.P.N. Rao, Tau-derived-hexapeptide ^{306}VQIVYK^{311} aggregation inhibitors: nitrocatechol moiety as A pharmacophore in drug design, ACS Chem. Neurosci. 4 (2013) 1559–1570.

[49] T. Silva, T. Mohamed, A. Shakeri, P.P.N. Rao, P. Soares da Silva, F. Remiao, F. Borges, Repurposing nitrocatechols: 5-Nitro-α-cyanocarboxamide derivatives of caffeic acid and caffeic acid phenethyl ester effectively inhibit aggregation of tau-derived hexapeptide AcPHF6, Eur. J. Med. Chem. 167 (2019) 146–152.

[50] S.A. Sievers, J. Karanicolas, H.W. Chang, A. Zhao, L. Jiang, O. Zirafi, J.T. Stevens, J. Munch, D. Baker, D. Eisenberg, Structure-based design of non-natural amino-acid inhibitors of amyloid fibril formation, Nature 475 (2011) 96–100.

[51] J. Zheng, C. Liu, M.R. Sawaya, B. Vadla, S. Khan, R.J. Woods, D. Eisenberg, W.J. Goux, J.S. Nowick, Macrocyclic β-sheet peptides that inhibit the aggregation of a tau-protein-derived hexapeptide, J. Am. Chem. Soc. 133 (2011) 3144–3157.

[52] L.P. Jameson, N.W. Smith, S.V. Dzyuba, Dye-binding assays for evaluation of the effects of small molecule inhibitors on amyloid (abeta) self-assembly, ACS Chem. Neurosci. 3 (2012) 807–819.

[53] M. Frenkel-Pinter, S. Tal, R. Scherzer-Attali, M. Abu-Hussien, I. Alyagor, T. Eisenbaum, E. Gazit, D. Segal, Naphthoquinone-tryptophan hybrid inhibits aggregation of the tau-derived peptide PHF6 and reduces neurotoxicity, J. Alzheimer's Dis. 51 (2016) 165–178.

[54] A. Paul, G.K. Viswanathan, S. Mahapatra, G. Balboni, S. Pacifico, E. Gazit, D. Segal, Antagonistic activity of naphthoquinone-based hybrids toward amyloids associated with alzheimer's disease and type-2 diabetes, ACS Chem. Neurosci. 10 (2019) 3510–3520.

[55] A. Micsonai, F. Wien, L. Kernya, Y.H. Lee, Y. Goto, M. Refregiers, J. Kardos, Accurate secondary structure prediction and fold recognition for circular dichroism spectroscopy, Proc. Natl. Acad. Sci. 112 (2015) E3095–E3103.

[56] C.L. Moore, M.H. Huang, S.A. Robbennolt, K.R. Voss, B. Combs, T.C. Gamblin, W.J. Goux, Secondary nucleating sequences affect kinetics and thermodynamics of tau aggregation, Biochemistry 50 (2011) 10876–10886.

[57] C. Wallin, Y. Hiruma, S. Warmlander, I. Huvent, J. Jarvet, J.P. Abrahams, A. Graslund, G. Lippens, J. Luo, The neuronal tau protein blocks *in vitro* fibrillation of the amyloid-beta (abeta) peptide at the oligomeric stage, J. Am. Chem. Soc. 140 (2018) 8138–8146.

[58] A. Crowe, C. Ballatore, E. Hyde, J.Q. Trojanowski, V.M. Lee, High throughput

screening for small molecule inhibitors of heparin-induced tau fibril formation, Biochem. Biophys. Res. Commun. 358 (2007) 1–6.
[59] S.C. Sahu, M. Amankwa-Sakyi, M.W. O'Donnell Jr., R.L. Sprando, Effects of usnic acid exposure on human hepatoblastoma HepG2 cells in culture, J. Appl. Toxicol. 32 (2012) 722–730.
[60] U.K. Hanisch, H. Kettenmann, Microglia: active sensor and versatile effector cells in the normal and pathologic brain, Nat. Neurosci. 10 (2007) 1387–1394.
[61] N. Zilka, Z. Stozicka, A. Kovac, E. Pilipcinec, O. Bugos, M. Novak, Human misfolded truncated tau protein promotes activation of microglia and leukocyte infiltration in the transgenic rat model of tauopathy, J. Neuroimmunol. 209 (2009) 16–25.
[62] B.P. Carreira, M.I. Morte, A.I. Santos, A.S. Lourenco, A.F. Ambrosio, C.M. Carvalho, I.M. Araujo, Nitric oxide from inflammatory origin impairs neural stem cell proliferation by inhibiting epidermal growth factor receptor signaling, J. Neuroimmunol. 8 (2014) 343.
[63] Y.Q. Cui, L.J. Zhang, T. Zhang, D.Z. Luo, Y.J. Jia, Z.X. Guo, Q.B. Zhang, X. Wang, X.M. Wang, Inhibitory effect of fucoidan on nitric oxide production in lipopolysaccharide-activated primary microglia, Clin. Exp. Pharmacol. Physiol. 37 (2010) 422–428.
[64] P.K. Kamat, S. Rai, S. Swarnkar, R. Shukla, S. Ali, A.K. Najmi, C. Nath, Okadaic acid-induced Tau phosphorylation in rat brain: role of NMDA receptor, Neuroscience 238 (2013) 97–113.
[65] O.A. Luzina, M.P. Polovinka, N.F. Salakhutdinov, G.A. Tolstikov, Chemical modification of usnic acid 2. Reactions of (+) - usnic acid with amino acids, Russ. Chem. Bull. 56 (2007) 1249–1251.
[66] Z. Khosravi, M.A. Nasiri Khalili, S. Moradi, R. Hassan Sajedi, M. Zeinoddini, The molecular chaperone artemin efficiently blocks fibrillization of TAU protein *in vitro*, Cell J. 19 (2018) 569–577.
[67] Q. Chen, Y. Du, K. Zhang, Z. Liang, J. Li, H. Yu, R. Ren, J. Feng, Z. Jin, F. Li, J. Sun, M. Zhou, Q. He, X. Sun, H. Zhang, M. Tian, D. Ling, Tau-targeted multifunctional nanocomposite for combinational therapy of alzheimer's disease, ACS Nano 12 (2018) 1321–1338.